Journal of Hydrology 676 (2026) 135681



Contents lists available at ScienceDirect

Journal of Hydrology

journal homepage: www.elsevier.com/locate/jhydrol





High resolution river and estuarine water level topography from nadir altimetry

Luciana Fenoglio[a,b,*], Jiaming Chen[a], Stefano Vignudelli[c], Ron Abileah[d], Elena Zakharova[e], Marco Restano[f], Jerome Benveniste[g], Jürgen Kusche[a]

[a] Institute of Geodesy and Geoinformation, University of Bonn, Bonn, 53115, Germany
[b] Department of Physics and Astronomy, Chalmers University of Technology, Gotheburg, 41296, Sweden
[c] CNR, Pisa, Italy
[d] jOmegak, San Carlos, I-00044, USA
[e] Maynooth University, Maynooth, Ireland
[f] ATG-Europe c/o ESA-ESRIN, Largo Galileo Galilei, Frascati, 1-00044, Italy
[g] ESA, Largo Galileo Galilei, Frascati, I-00044, Italy

HIGHLIGHTS

- Best accuracy of 10 cm in rivers with FFSAR 80/140 Hz and SAMOSA+ retracker.
- Highest improvement in accuracy at the coast and in small reservoirs with FFSAR vs UFSAR.
- Higher accuracy of water level from SWOT than from nadir-altimetry over all targets.

ARTICLE INFO

This manuscript was handled by Ashok Mishra, Editor-in-Chief

Keywords:
Radar nadir-altimetry
Fully-focused SAR
Unfocused SAR
Water surface elevation
Hydrological topography

ABSTRACT

Standard unfocused Synthetic Aperture Radar (UFSAR) nadir-altimeter products with a posting rate of 20 Hz provide water level heights with an along-track spacing of 300 meters, which is far from being optimal for coastal zone and inland studies. The fully focused FFSAR processing, which allows much higher resolution and posting rate, shall resolve small scales interferences along-track and thus improve the accuracy and precision of the geophysical estimates. This study looks at different water surfaces in rivers, lakes and coastal zones to investigate under which conditions and processing schemes the accuracy of water level measurements is higher with FFSAR rather than with UFSAR. We focus on Sentinel-3A, -3B and -6A missions during 2016–2023. Starting from the UFSAR products at a 20 Hz posting rate, we investigate the optimal choice for the Level 1 to Level 2 processing algorithms and parameters. We find that posting rates of 80 Hz for Sentinel-3 and 140 Hz for Sentinel-6 are best suited for all inland targets. Our results indicate that the FFSAR, combined with the SAMOSA+ physical retracker, is likely to provide the highest accuracy and the largest number of observations for all targets, with averages of 15–20 cm in rivers, 6 cm in lakes, 40 cm in estuaries and 10 cm at the coast. The gain in accuracy of FFSAR over UFSAR is, for the same posting rate and retracker, smaller than 5 %, except for small targets with river widths smaller than 100 meters, areas smaller than 0.1 km^2 and proximity to the coast. This study recommends FFSAR processing, although nadir-altimetry does not deliver longitudinal river profiles all along the river. Where water surfaces decorrelate quickly over time, the FFSAR accuracy may degrade, with a more pronounced impact over the open ocean compared to lakes.

1. Introduction

Changes in surface water are monitored today globally by altimeter satellites, from laser-based systems with Icesat-2 to radar single antenna systems with Sentinel-3/6, radar interferometry with CryoSat-2 and radar swath-interferometry with SWOT. To capture the space-time variability of water, temporal revisit, spatial coverage, spatial resolution, accuracy, and latency time have to be optimized (Cerbelaud et al., 2025). While the temporal revisit of 90 days for Icesat-2 is optimized for

* Corresponding author at: Department of Physics and Astronomy, Chalmers University of Technology, Gotheburg, 41296, Sweden.
Email address: lucfen@chalmers.se (L. Fenoglio).

https://doi.org/10.1016/j.jhydrol.2026.135681
Received 2 October 2024; Received in revised form 21 April 2026; Accepted 11 May 2026
Available online 12 May 2026
0022-1694/© 2026 The Authors. Published by Elsevier B.V. This is an open access article under the CC BY license (http://creativecommons.org/licenses/by/4.0/).

ice surfaces, nadir-radar altimeters have been monitoring global water heights since 1992 with a temporal revisit between 10 and 29 days. Land contamination significantly affects low resolution mode (LRM), degrading both the altimetric range and the geophysical corrections in the last 5 km from the coast and inland waters (Biancamaria et al., 2016). The water level observations from space have a decimeter accuracy and the coverage is limited to 15 % of the lakes and rivers due to the characteristics of the mission (Benveniste et al., 2019; Schröder et al., 2019). The accuracy depends on the instrument, area and shape, surroundings and retracking method. For nadir-altimeters with higher pulse repetition frequency (PRF), the SAR and SARIN processing, also called Unfocused SAR (UFSAR), provides along-track water level measurements at higher spatial resolution than in LRM (Egido and Smith, 2017). UFSAR uses both the phase and power of nadir and non-nadir along-track pulses to increase the number of observations of a given point on the ground, the range delay correction of non-nadir pulses is applied in the time domain. The UFSAR algorithm applies coherent processing to the 64 echoes within each burst (equivalent to 3.5 ms of flight) through an along-track fast Fourier transform (FFT). With pulses transmitted at a PRF of 18 kHz, the 64 resulting Doppler bins have a bandwidth of about 280 Hz, which leads to a resolution of about 320 m in the along-track direction. The typical UFSAR posting rate is 20 Hz, which corresponds to the along-track resolution and ensures a minimum overlap between footprints of adjacent waveforms (Egido et al., 2021). By increasing the conservative UFSAR posting rate to 80 Hz in Sentinel-3 and 140 Hz in Sentinel-6, the noise of the estimated geophysical parameters can be reduced and this has a physical justification based on the correlation properties of the multi-looked SAR waveforms Ehlers et al. (2023b). In UFSAR the maximum resolution is around 300 meters, and the highest possible posting rate is 80/140 Hz which leads to a separation between two points on the Earth's surface of 80 meters and 50 meters respectively (Dinardo et al., 2021).

The FFSAR processing technique (Egido and Smith, 2017) allows achieving high resolution and accuracy from nadir altimetry data, by performing fully-focused coherent processing of pulse echoes from a nadir-looking pulse-limited radar altimeter. In theory, FFSAR allows an along-track spatial resolution of up to 0.5 meters for an integration time of 2 seconds. The posting rate of multi-looked waveforms influences the signal-to-noise ratio and speckle noise. Amraoui et al. (2024) propose multi-looking, which consists in spatial averaging of FFSAR to achieve noise reduction while preserving high resolution. In this way FFSAR can mitigate small-scale interferences in the along-track direction and thus improve the accuracy and precision of the geophysical estimates. Several studies have used FFSAR comparing UFSAR and FFSAR methodologies and results (Ehlers et al., 2023a; Egido et al., 2021; Schlembach et al., 2023; Amraoui et al., 2024; Domingo et al., 2025). Kleinherenbrink et al. (2020) applies FFSAR on the CryoSat-2 altimetry for monitoring water surfaces at the coast, whereas other studies investigate the benefits of FFSAR processing applied to Sentinel-6 for inland water levels of small reservoirs (Domingo et al., 2025) and to coastal wave height estimates citepSchlembach2023. FFSAR requires a higher computational effort than UFSAR when the focusing algorithm back-projection (BP) is applied (Egido and Smith, 2017). BP applies the phase range correction of non-nadir pulses in the time domain and, due to the longer integration time, the phase range correction of non-nadir pulses should be taken into account more precisely than in UFSAR. In contrast, the Omega-Kappa (WK) algorithm applies it in the frequency domain (Guccione et al., 2018) and requires a much shorter computation time (Guccione et al., 2018; Hernández-Burgos et al., 2024). Recently, FFSAR processing of nadir-altimetry was applied to off-nadir water targets to enhance the spatial density of the observations and thus the accuracy of the derived water level for suitable relative configurations of the altimeter tracks and the water body (Chen et al., 2025; Ehlers et al., 2025; Nguyen et al., 2025).

In addition to new processing algorithms, other changes in the altimetric mission design, such as the open burst approach and the open loop tracking command (OLTC), have improved the ability to obtain valid measurements in the inland water domain. The interleaved (open burst) transmit and receive approach improves the altimeter noise characteristics of Sentinel-6 due to the higher number of looks (Donlon et al., 2021). The OLTC allows since 2016 the observation of more inland water targets with Jason-3 and Sentinel-3 (Le Gac et al., 2021). SAR Interferometry (SARin) which uses two antennas to observe across-track non-nadir targets mitigates land contamination signals, as was first observed with CryoSat-2 (Abulaitijiang et al., 2015).

In single-antenna nadir altimeters, since 2010 with CryoSat-2, land contamination has been reduced by increasing the pulse repetition frequency (PRF) by a factor of 10 from Low Resolution Mode (LRM) to High Resolution Mode (SAR). Compared to SAR mode, in LRM mode the main limitation is the land contamination. Rivers narrower than 100 m and lakes smaller than 1 km^2 are not observed and the accuracy for large rivers is 0.30 m, while for medium size rivers it is 0.30–0.70 m with ENVISAT and 0.30 m with Jason-2,-3 (Schwatke et al., 2015). In coastal zones, data are masked at distances smaller than 7–10 km from the coast. CryoSat-2 has used, since 2010 three geographical masks: Low Resolution (LRM) over land and open sea, SARIn in mountainous and river regions and SAR mode in coastal and estuarine regions. Sentinel-3 has non-simultaneous LRM and SAR modes and operates globally in SAR mode. Sentinel-6A has measured, since 2020 simultaneously in interleaved SAR and LRM modes. Compared to the km-large footprint in LRM mode, SAR and SARIn modes have a finer along-track resolution of 350 m. Altimetry in SAR mode has demonstrated higher accuracy and precision compared to LRM. Fenoglio et al. (2021) and Dinardo et al. (2021) report on an accuracy against in-situ data of 4 cm in the coastal zone, while Rulent et al. (2020) report on an improved agreement between satellite altimetry and ocean numerical models at distances greater than 3–4 km from the coast. The accuracy of water level in inland water ranges from a few centimetres to decimetres depending on the altimeter mode, retracking method, orientation of the ground track relative to the riverbed, modeling of the hooking effects and tropospheric correction (Boergens et al., 2016; Halicki et al., 2023).

The swath-altimetry radar interferometry mission SWOT, launched in December 2022 by NASA and CNES, starts a generation of satellite missions mapping the Earth's water surfaces with unprecedented resolution and coverage. On the ocean it resolves sub-mesoscale features and eddies that nadir tracks miss (Desai, 2018; Peral et al., 2024; Verger-Miralles et al., 2025; Archer et al., 2025) and on land it shows realistic values of slopes of unprecedented resolution for application to fluvial geomorphology dynamics and erosion (Normandin et al., 2024).

In this manuscript we compare water level products obtained with fully-focused and unfocused processing on different types of water surfaces. In Section 2 we present the study areas and data used. We have selected rivers, lakes and coastal areas in Europe and use standard and in-house developed products for Sentinel-3A/3B and Sentinel-6A. The in-house product uses the Omega-Kappa algorithm which requires less computation time. In Section 3 the methodology is described for the WK algorithm, for creating the time-series and for evaluating their accuracy. In Section 4 the FFSAR time-series of water level created in Section 3 are compared to UFSAR and in-situ data. Section 5 presents a discussion of the results in Section 4 and compares the FFSAR against other time-series derived from the Precision Inland Surface Altimetry (PISA) (Abileah and Vignudelli, 2021) and from the SWOT mission. Section 6 summarizes the conclusions.

2. Materials

2.1. Study area

For the large amount of in-situ data, the river Rhine and its tributaries between Lake Constance and the Dutch border are an excellent case of a river system, lakes in Switzerland are selected as examples of lakes and reservoirs, and the Elbe estuary and the German coast are selected for the coastal analysis (Fig. 1).

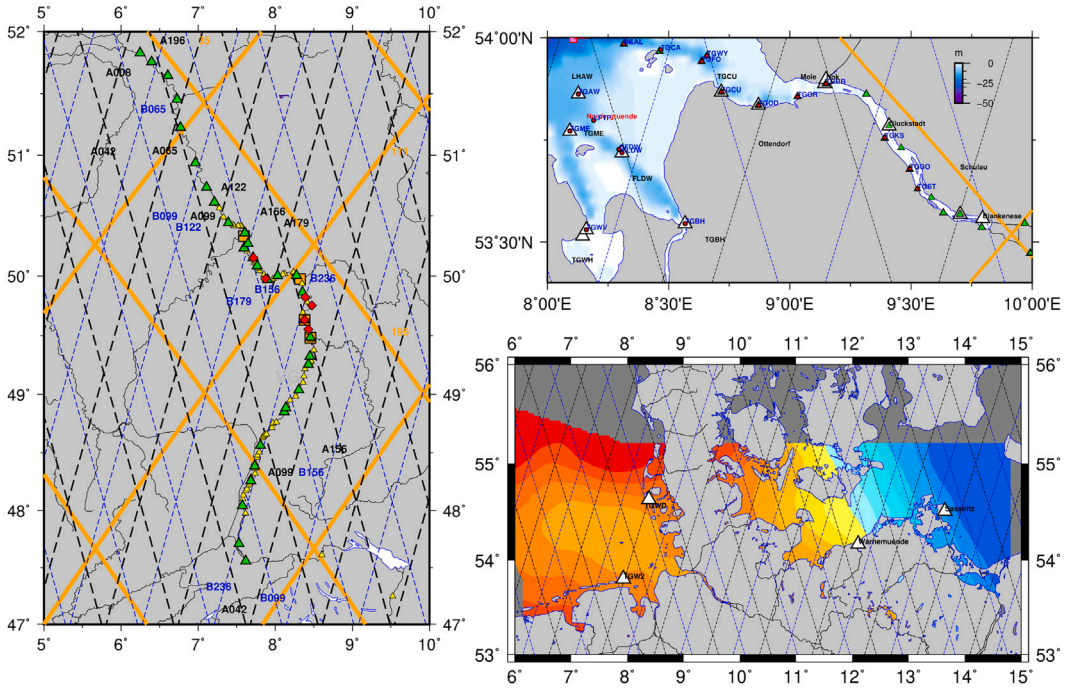


Fig. 1. Region of interest: River Rhine (left), Elbe River (top right), coastal zone (bottom right). WSV in-situ gauges (triangles), Sentinel-3A (black), Sentinel-3B (blue) and Sentinel-6 (orange). (For interpretation of the references to colour in this figure legend, the reader is referred to the web version of this article.)

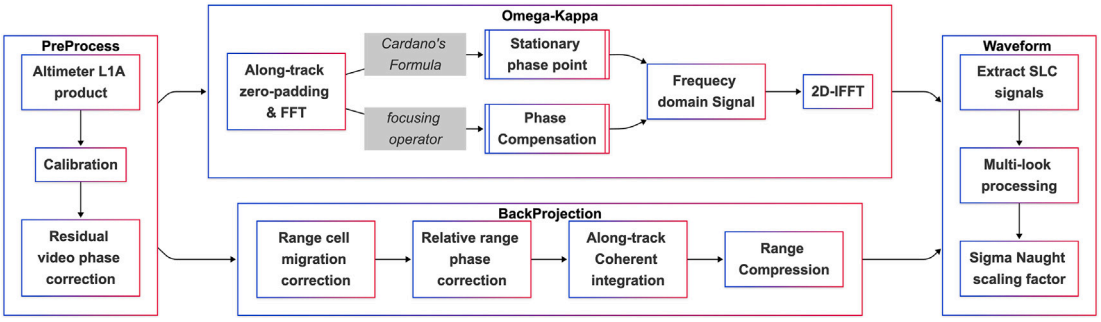


Fig. 2. Flowchart of FFSAR processing using Omega-Kappa and Backprojection.

2.2. Data

2.2.1. Nadir altimeter data

The Sentinel-3A and -3B data have been available since 2016 and 2018, respectively, while the Sentinel-6 data have been available since 2020. We use for Sentinel-3 the UFSAR products from the Copernicus standard (Cop), the land thematic products (CopHY), and the SARvatore service of the Earth Console Altimetry Virtual Lab (AVL) (https://earthconsole.eu/altimetry-virtual-lab/) as well as in-house UFSAR and FFSAR products. For Sentinel-6, we use the UFSAR products from EUMETSAT along with in-house UFSAR and FFSAR products. All Copernicus standard and thematic products for Sentinel-3 and Sentinel-6 have a 20 Hz posting rate. In the processing Hamming windows applied to burst data and zero-padding applied to the echoes are not applied consistently: none is applied in the official products, only zero-padding is applied in the official Sentinel-6 products, and both are applied in the Sentinel-3 land-thematic products. We have chosen to apply both the Hamming window and zero padding to the AVL UFSAR products at an 80 Hz posting rate, as in Dinardo et al. (2018). We make the same choice for the in-house processed products, for which different posting rates have been selected. In the processing from Level 1b to Level 2, in standard Cop and thematic CopHY the waveforms are retracked with the SAMOSA (Ocean) and the OCOG algorithms. The SAMOSA + (samp) algorithm (Dinardo et al., 2018) is chosen for the AVL products. We select for in-house UFSAR and FFSAR several algorithms, including the Ocean, OCOG, PTR, Multi-PTR (mptr) and the SAMOSA + algorithms. The Hamming weighting window applied to the burst data mitigates the effects of side-lobe ambiguities and the impact of ghost signals originating from very high scattering targets placed outside the main-lobe of the synthetic beam. After beam-forming and beam-steering are applied to form the fan of synthetic Doppler beams and to make the Doppler footprints co-located with the surface sample locations, an FFT zero-padding over-sampling the return radar waveform by a factor of two is applied to sample very peaky echoes from bright targets. The double extension of the receiving window mitigates the on-board tracker errors on rough topography.

We consider the altimeter L2 products generated in the HYDROCOASTAL project (https://eo4society.esa.int/projects/hydrocoastal), which aimed at maximising the exploitation of SAR and SARIn altimeter measurements for the Sentinel-3 and CryoSat-2 missions. Various processing algorithms for SAR altimetry in coastal zones and inland waters were developed. In case studies the various products were inter-compared and compared to other products. We

use three of them for inland water, HYATK, HYDTU, and HYISR, and four for coastal areas, HYDTU, HYISR, HYTUM, and HYBonn. Below the retrackers are briefly described. The HYATK is an Empirical Retracker developed to address the non Brownian radar altimeter echoes, and is dedicated to multi-peak data acquired in continental hydrology. The HYDTU (MWaPP) (Multi-Waveform Persistent Peak) empirical retracker uses all the waveforms extracted over a water body to derive the sub-waveform containing the nadir information, this is retracked with a standard threshold retracker (Villadsen et al., 2016). The HYISR 2-step retracker is a modification of the analytical retracker SAMOSA (Ray et al., 2015) implementing a two-step fitting procedure to operate over both coastal and inland waters (Gao et al., 2019). The HYTUM sub-waveform retracker ALES+ SAR (Adaptive Leading Edge Subwaveform retracker for SAR) is an evolution of the ALES+ algorithm developed for conventional altimetry in Passaro et al. (2018). The HYBonn sub-waveform retracker Spatio-Temporal Altimeter Retracker for SAR altimetry (STARS) combines a processing scheme (STAR) for conventional altimetry (Roscher et al., 2017) with the Signal model Involving Numerical Convolution for SAR (SINCS) developed for Delay Doppler altimetry (Buchhaupt et al., 2018). It consists of three steps: partitioning into sub-waveforms, retracking with SINCS, and selection of one estimate with a shortest-path algorithm under the assumption of similarity of estimates at successive along-track positions. Alternative processing is performed with an in-house FFSAR processor using the Omega-kappa algorithm and the SAMOSA+ retracker (Dinardo et al., 2018).

2.3. SWOT altimeter data

The SWOT mission employs a wide-swath measurement technique. This study uses SWOT version C Level-2 products from three distinct datasets: SWOT PIXC, SWOT Raster and L3 Low Resolution products.

The SWOT PIXC (Pixel Cloud) data is a high-resolution, sparse point cloud dataset (5–10 m along-track) representing classified water pixels. It provides geolocated heights, backscatter intensity, and essential quality flags for water bodies. We keep pixels classified as open water (classification = 4) and apply the geolocation, interferogram, and σ_0 quality flags, excluding all pixels with flag values greater than zero. The SWOT Level 2 High Rate (HR) Raster product resamples irregular, high-resolution pixel clouds and provides mapped water surface elevation, inundation extent, and radar backscatter. We use the 100 m uniform grids. We apply the quality flag to keep only the observations classified as good (wse = 0). The SWOT L3 Low-Resolution (LR) Unsmoothed product is a 250-meter dataset providing ocean topography. Unlike the standard 2-km L3 product, the unsmoothed version retains the full 250 m resolution of the Level-2 data, offering crucial high-resolution data for coastal, eddy, and geophysical applications. We retain only data at a distance to the coast equal to or larger than 2 km, we find this choice suitable to avoid coastal noise. The SWOT pixel clouds SWOT-PIXC (v2.0) and SWOT Raster are available at PODAAC (https://podaac.jpl.nasa.gov/dataset/SWOT_L2_HR_PIXC_2.0 and https://podaac.jpl.nasa.gov/dataset/SWOT_L2_HR_Raster_2.0), and the SWOT L3 Low Resolution unsmoothed product is available at AVISO+ (https://www.aviso.altimetry.fr).

2.3.1. Gauge station data

In-situ water level data are available in Germany from the National Hydrological Agencies (Bundesanstalt für Gewässerkunde (BfG)) and the Waterways and Shipping Administration Wasser Schifffahrt Verwaltung (WSV) with a maximum frequency of 15 minutes. The time-series of water level heights are measured relative to the zero point of the gauge (PNP), whose height is available in the German reference height system DHHN2016 (http://www.pegelonline.de). The transformation to the ITRF Reference System 2014 for the epoch 2021 (01.01.2021) is performed in two steps. First the heights are transformed from DHHN2016 to ETRS89/DREF91/R16 by adding the quasigeoid GCG2016 (http://gibs.bkg.bund.de/geoid/gscomp.php?p=g). Then the transformation from ETRS89/DREF91/R16 to ITRF2014 (epoch 2021) is provided by the Arbeitsgemeinschaft der Vermessungsverwaltungen der Länder der BundesrepublikDeutschland (AdV) and applied at BfG, which provides the ellipsoidal heights of the PNP in the ITRF2014. In Switzerland, the in-situ water level data distributed by the National Hydrological Agencies (BAFU) with a maximum frequency of 15 cm are measured relative to the CH geoid. The transformation from the CH geoid to the GRS80 ellipsoid is provided online (https://www.swisstopo.admin.ch/en/coordinates-conversion-navref). The CHGeo2004 geoid model, which was computed by the Federal Office of Topography (Swisstopo) was the official geoid model from 1998 to 2004.

3. Methods

3.1. FFSAR processing and waveform retracking

FFSAR coherently focuses on subsequent along-track surface points, separated by a selectable distance. The processing operates over a data block, composed of a number of bursts, that is shifted along the bursts of the input file to process the data sequentially. The size in number of bursts of the data block defines the extension of the synthetic aperture of the FFSAR processing, called illumination time. During the focusing process, each data block leads to the generation of a single-look on the ground that is aligned with the center of the data block. Subsequent single looks are equally spaced in time by the Pulse Repetition Interval (PRI). The single-looks are spatially averaged in power to obtain multi-looks. The sampling frequency, called posting rate, defines the number of single-looks that are multi-looked in the multi-looking step. For a given Level-1A product, we process sequentially data blocks of 180 bursts, corresponding to an illumination time of 2.3 s, until all bursts of the product are processed. Two subsequent data blocks are shifted relative to one another by a predefined amount, named shifting, of 4 bursts. The single-looks generated for each data block correspond to one radar cycle. The single-looks are centred around the central burst of a data block, they do not overlap between subsequent data blocks and a continuity in ground coverage is guaranteed.

A FFSAR processing using the Omega-Kappa (WK) SAR focusing algorithm (Guccione et al., 2018) was implemented by extending the open source code package SMAP provided by CLS in the SMAP FFSAR CLS ESA project (https://doi.org/10.5270/esa-cnes.sentinel-3.smap) (SMAPEBo). See Fig. 2 for the comparison with the original code in a flowchard. SMAP implements for Sentinel-3 the FFSAR processing with the time-domain back-projection algorithm (BP) and the two retrackers OCOG (Offset Center of Gravity) and MultiPTR (Davis, 1997). We find that the WK algorithm significantly speeds up the FFSAR processing, reducing the computing time to 1/10 of the time needed by the BP algorithm using multi-threading. For a fair comparison of the UFSAR and FFSAR processing, the retracker SAMOSA+ (Dinardo et al., 2018) was implemented to extract the geophysical parameters in the open source code package SAMPY (https://github.com/cls-obsnadir-dev/SAMPy). During FFSAR processing, a zero-padding factor of 2 is applied to enhance the sampled frequency of the waveform. Additionally, an azimuth Hamming window is applied to Sentinel-3, while no Doppler window is applied to Sentinel-6. Finally, multilooking is performed at 80 Hz for Sentinel-3 and 140 Hz for Sentinel-6 to reduce the impact of speckle noise, resulting in along-track resolutions of 110 meters and 63 meters, respectively with a value of 8441 m/s for the satellite velocity projected on the ground.

Details on the processing scheme and computation time are given below for completeness. The computing time for central Europe was less than one day. The processing of Sentinel-3 and Sentinel-6 from Level 1A to Level 2 was run at the Jülich Supercomputing Centre (JSC) in two steps, the first SMAPEBo performing the UFSAR/FFSAR focusing and the second SAMPEBo performing the retracking. The computation time for a single track depends on the area, and is 6 hours for a selection between

35 and 71 degrees latitude. Choosing the WK algorithm allowed a reduction by a factor of 60 in the time needed by the BP algorithm for a single track. We ran SMAPEBo in parallel for each single ground-track over all cycles, which are 105 and 75 for Sentinel-3A and Sentinel-3B in 2016–2023. Selecting a number of tasks equal to the number of cycles and CPUs per task equal to 4, we processed 12 tasks per node and needed 9 nodes. SMAPEUBo also performs the UFSAR processing and the computing time was 1.5 larger than for WK FFSAR. In the retracking step SAMPEUBo, the SAMOSA+ retracker runs over all cycles for each ground track. The simple parallelisation plan made over the ground tracks consists of using a node for each (external) input directory (track). The L2 files are processed sequentially in each of the input directories and the multi-processing of a single file/track uses all cores in a node with 96 CPUs-per-tasks. The number of nodes is selected equal to the number tracks. The processing in a single node, for a single track was of 10 hours and the parallel run lasted 10 hours.

3.2. Building time-series of water heights from satellite altimetry

Different approaches have been used to produce the Once per Crossing (OPC) measurements at the Virtual Gauge (VG) position. To select the nadir along-track points located in the river, a static or a variable river mask based on land-water masks is needed. We first considered the occurrence from the Global Surface Water Explorer (https://global-surface-water.appspot.com) (Pekel et al., 2016) which is based on Landsat images from the period 1984 to 2018 and has a resolution of 30 m. Alternatively the static width available in the SWORD database was used (Altenau et al., 2021). We finally select for the Rhine the static mask provided by the German Federal Institute of Hydrology (BfG), which agrees well with the 90 % percentage of water occurrence in Pekel et al. (2016). The VG location is selected at the intersection of the reference satellite tracks with the river centerline, another choice is the node in the SWORD database that is nearest to the most of observations for all cycles. The single observations are then corrected by the slope of the river between the actual location and the VG location. The slope value used is extracted from the SWORD database and is constant over time. Time-series from nadir-altimetry in the river are built by the Virtualpass method by collecting the mean value of the water heights retained in each cycle. All types of surfaces found within the water body crossing are aggregated into a single water height measurement. The merging can result in noisy time-series. We filter the time-series for outliers using a recursive 4 sigma rejection filter. Nielsen et al. (2022) use a state-space model where the process part is a first-order auto-regressive process to combine the data in a reach. The density of measurements or Sampling Loss Rate is accounted for in the validation exercise as various retrackers result in different numbers of retained points in the time-series.

To build time series in estuaries, at the coast and in a lake, the nadir-altimeter observations are averaged over a given radius or over a selected area. When the area is small compared to the track distance, we say that data are binned along the repeat track. In the estuary and in the lake we use data binned at 20 Hz along-track (~ 300 meters). In rivers and estuaries, with SWOT PIXC, the variable slope is estimated assuming that the surface is linear. For a given site, we consider the pixels located within 1 km upstream and downstream along the river centerline and we model the WSE_i at pixels i as a linear function of the along-river distance ss_i between the measurement point and the given site. The slope $\hat{s}$ and the WSE $\hat{h}$ over the selected 2 km pixels are derived from the linear model in a weighted least squares linear regression approach JPL D-56411, Revision C (2025).

$$\mathrm{wse}_i = s \cdot \mathrm{ss}_i + h + \epsilon_i \quad (1)$$

To discuss the comparison between nadir-altimetry and SWOT in the lakes we build the two time-series as described below. Over a lake, nadir-altimetry observations from different orbital tracks and satellite platforms exhibit distinct temporal sampling characteristics and systematic biases. Therefore, to generate a consistent, high temporal-resolution water level time series for that lake, we use the fusion algorithm based on an adaptive Kalman filter with explicit bias estimation Schwatke et al. (2015). Using SWOT, all Raster valid grid points covering the lake are first referred to the local geoid. Specifically, the observed water surface elevation is corrected using the local geoid models GCG2016 and CHGeo2004. Subsequently, the corrected grid points are aggregated within the corresponding lake mask contained in the Prior Lake Database (PLD) (Wang et al., 2025) using a median spatial clustering approach, where the lake water surface elevation is estimated as the median of the set of valid grid points falling within the corresponding lake mask.

3.3. Evaluating water level elevation observations

The statistical parameters average (mean and median) and standard deviation of differences (STDD) have been evaluated from pairs of VG and their nearest real gauges within 30 kilometers. The two parameters reflect the bias and accuracy of the altimeter measurements and are affected by river characteristics, such as width and orientation. Several in-situ stations are merged together to produce more robust statistics in boxplots. On each box, the central mark indicates the median, and the bottom and top edges of the box indicate the 25th and 75th percentiles, respectively. The whiskers extend to the most extreme data points not considered outliers, and the outliers are plotted individually using the cross marker, in Figs. 4 and 5. Confidence intervals and p-values are estimated to evaluate the significance of the differences between the results obtained from FFSAR and USAR. We use the *t*-test and the ANOVA test. A significant difference is found for $p < 0.05$.

Investigation of the correspondence between Level 1 radargrams and Level 2 time-series gives insight into differences between LRM, UFSAR and FFSAR nadir-processing and thus into the expected data quality (Figures from Figs. 7–9). The analysis is described in the next section.

4. Results

4.1. Rhine river

The Rhine River has been selected due to the high density of in-situ data available for the validation of the nadir-altimeter water heights. Fig. 3 shows the time-series and the statistics of the comparison against the in-situ station of Mainz. The STDD of 9 cm is the lower limit achievable in this area with our methodology. It is particularly interesting to understand what is still contained in the time series of differences. The dependence of the STDD on the track-river orientation is seen in Fig. S1 for the forty-two virtual gauges (VG) of Sentinel-3. The boxplots of the STDD between in-situ and altimetric water time-series have been built for several L2 products at pairs of virtual gauges and nearest real stations within 30 kilometers. We see in Fig. S1 that the STDD depends on the orientation of the track and not on the width of the river. We cluster the UFSAR product distinguishing between the 20 Hz products generated in the Hydrocoastal Project, the Copernicus 20 Hz products and the AVL on-demand. Over 42 stations, among the L2 Hydrocoastal products, DTU performs best with a median of 0.3 m, while the mean is 0.9 m. The L3 DTU time-series have a lower mean of the STDD (0.47 m) (Table 1, Fig. 4a). Among the Copernicus products and over the same 42 stations, the thematic product (CopHY) with the SAMOSA ocean retracker gives the smallest mean STDD (0.67 m) (Table 2, Fig. 4b). Instead, the AVL SARvatore product with SAMOSA+ retracker, processed at an 80 Hz posting rate (AVLsamp) gives the smallest mean overall (0.48 m). We compare the FFSAR to UFSAR products over the 100 km long Rhine River section between Speyer and Mainz, where the Sentinel-3A track 156 intersects the river at several points. The STDD of DTU, UFSAMP at 20 Hz and FFSAMP at 80 Hz are given in Table 3, Fig. 4(c). FFSAR processing has the smallest mean and median and retains the highest number of points (Tables 4 and 5). We select the waveforms whose pulse peakiness is smaller than 0.4 and misfit error smaller than 8. Waveform selection in FFSAR increases the accuracy to 16 cm in FFSAR and to 17 cm in UFSAMP (Table 4, Fig. 4 d).

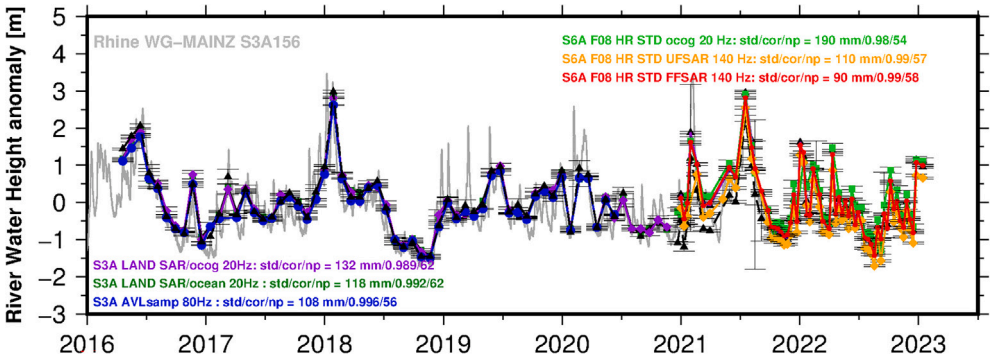


Fig. 3. Water level anomalies built by the Virtualpass method at the Sentinel-3 and Sentinel-6 VGs near Mainz along with statistics of comparison to the Mainz gauge.

Table 1
Sentinel-3: Mean and median of standard deviation difference (STDD) (m) between time-series at 48 VGs of Hydrocoastal level 2 and level 3 products and in-situ, Fig. 4(a).

STDD	HYATK 20 Hz	HYDTU 20 Hz	HYESA 20 Hz	HYISR 20 Hz	HYTUM 20 Hz	L3-HYDTU 20 Hz	L3-HYAHL 20 Hz
Median	0.485	0.325	0.394	0.338	0.354	0.247	0.265
Mean	0.813	0.926	0.671	0.691	0.795	0.475	0.776

Table 2
Sentinel-3: Mean and median of STDD (m) between time-series at 42 VGs of official and dedicated agencies products and in-situ, Fig. 4(b).

STDD	CopOce 20 Hz	CopOcog 20 Hz	AVLsamp 80 Hz	CopHYOce 20 Hz	CopHYOcog 20 Hz
Median	0.288	0.367	0.232	0.272	0.303
Mean	0.635	0.860	0.481	0.561	0.717

In rivers narrower than 100 m, such as the river Main in Frankfurt, Sentinel-6 FFSAR 80 Hz has an accuracy of 17 cm with a higher number of points than UFSAR and standard products, see Fig. 6(a). In regulated rivers the water level is maintained almost constant, as in Ottenheim, with an accuracy of 29 cm and an equal number of points for FFSAR, UFSAR and standard products (Fig. 6b). Analysing water levels above the reference ellipsoid WGS84, we find near Worms a bias of 40 cm in Sentinel-3 between FFsamp and the CopHY Thematic Products using the Ocean retracker (Fig. 6e). While this bias between the altimetric

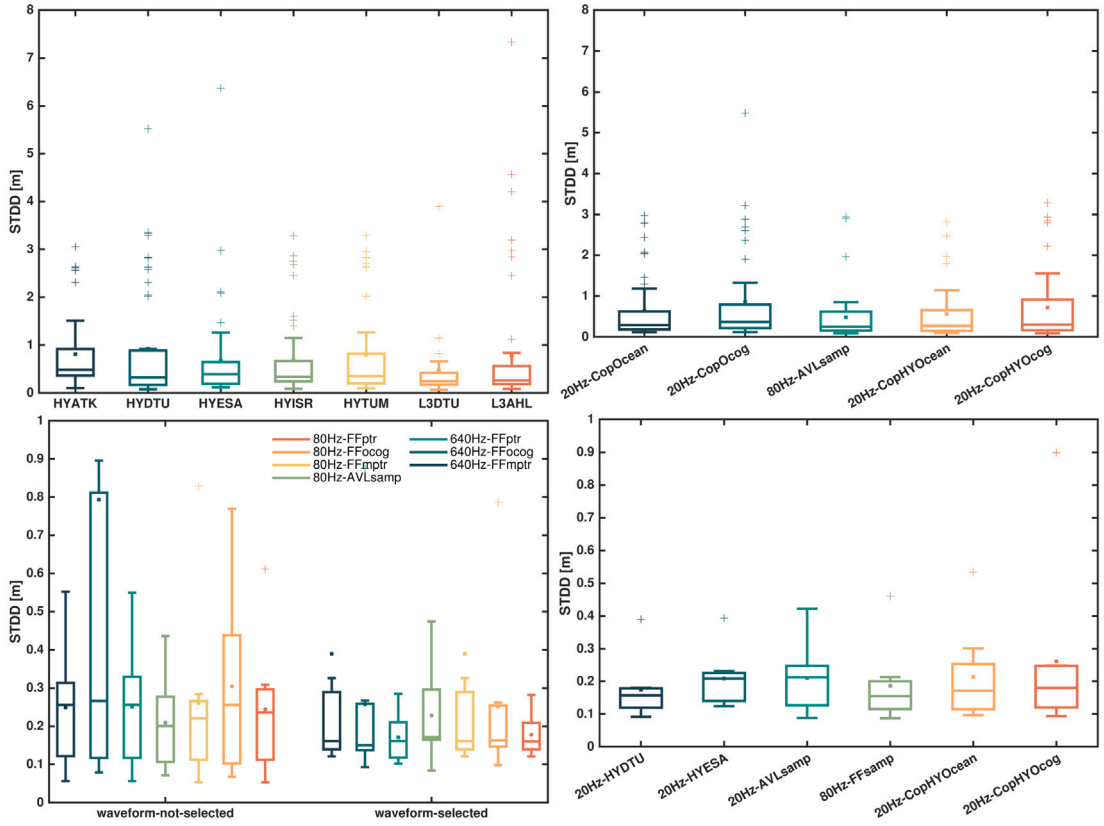


Fig. 4. Boxplots of STDD between altimetry and in-situ measurements in the River Rhine at (a) 48 VGs of Hydrocoastal Sentinel-3 level 2 and level 3, (b) 42 VGs of Earth Console SAMP 80 Hz, 20 Hz Copernicus standard and Copernicus thematic products for Sentinel-3, (c) 8 VGs of FFSAR Sentinel-3A with (right) and without (left) waveform selection for different posting rates and retrackers, (d) 8 VGs of HY, AVL, FFSAR and CopHY Sentinel-3A.

Table 3
Sentinel-3 Rhine: Mean and median STDD (m) between time-series at 8 VGs of FFSAR and UFSAR dedicated and Hydrocoastal product and in-situ, Fig. 4(c).

STDD	HYDTU 20 Hz	AVLsamp 20 Hz	FFsamp 80 Hz	CopHYOce 20 Hz	CopHYOcog 20 Hz
Median	0.157	0.212	0.155	0.171	0.180
Mean	0.174	0.210	0.186	0.213	0.261

Table 4
Sentinel-3 Rhine: Mean and median of the STDD (m) time-series at 8 VGs of FFSAR and of the AVL, without and with pre-selection of the waveforms, Fig. 4(d).

STDD	AVLsamp 80 Hz	FFmptr 80 Hz	FFocog 80 Hz	FFptr 80 Hz	FFmptr 640 Hz	FFocog 640 Hz
Median	0.201	0.221	0.256	0.236	0.256	0.266
Mean	0.209	0.260	0.304	0.244	0.249	0.794
Meanwfs	0.172	0.161	0.163	0.160	0.161	0.150

Table 5
Sentinel-6 Rhine: Mean and median of the STDD (m) of in-situ and altimeter time-series of in-house FFSAR, in-house UFSAR and official products, 4 VGs, Fig. 5(a).

STDD	FFsamp 140 Hz	UFsamp 140 Hz	EUMocog 20 Hz
Median	0.159	0.143	0.178
Mean	0.186	0.186	0.201

products is confirmed at other locations, no bias is found between FFSAR and in-situ data. In Fig. S4 the Sentinel-3 waveforms and the range gate of the FFSAR and UFSAR products using the SAMP retracker are very similar. Instead, the range gate of the CopHY UFSAR product, using the Ocean retracker, has a different range gate. We conclude that the bias depends on the retracker used.

For Sentinel-6 we consider four VGs in the Rhine and its tributary the Main River. FFSAR and UFSAR 140 Hz have the same mean while more points are retained in FFSAR. Comparison with the 20-Hz EUMETSAT standard products F08 shows that the OCOG retracker (EUMOcog) has lower accuracy and retains fewer points (Table 5, Fig. 5a), Figure S3.(a). The mean accuracies of 18 and 20 cm for FFSAR and EUMOcog agree with the accuracy of Sentinel-3, the accuracy of EUMOcog is lower than that of Sentinel-6. We argue that the accuracy of the time series is related to the quality of the radargrams. To illustrate the differences between radargrams, we focus on Rhine-km 503, see Fig. 7. Sentinel-3 Track 156 and Sentinel-6 Track A111 intersect the river between Wiesbaden and Mainz at 6 km from the Mainz gauge and Sentinel-6 overflies the Biebrich gauge. We explore the relationship between radargrams and time-series quality. There is a bright signal peak on the radargram at locations where the river is located at nadir. The STDD of the Sentinel-6 altimeter against the Mainz in situ water level is 9 cm, 11 cm and 19 cm for FFSAR 140 Hz, UFSAR 140 Hz and EUMOcog 20 Hz. The number of points retained by EUMOcog is 93 % of the points retained in FFSAR. The UFSAR radargram is smoother than the FFSAR radargram, where strong reflections are produced by ponds. Radargrams may be significantly different at different epochs, as shown for the two selected dates. The FFSAR and UFSAR waveforms collected at the mid-river location coincide only at the second epoch, see Fig. 7 (bottom right).

In the Rhine River, we compare the Sentinel-3 FFSAR and UFSAR results shown in Fig. 5(b). We find no significant difference in STDD between 80 Hz-FFsamp and 20 Hz-AVLsamp with p-value 0.163, and no significant difference between 80 Hz-FFsamp and 20 Hz-DTU with p-value: 0.38. Instead we find a statistically significant difference in STDD (p-value: 0.024) between the two UFSAR products of Hydrocoastal AVLsamp20Hz and HYDTU20Hz. Their mean difference (HYDTU20Hz - AVLsamp20Hz) is −0.036 and their Standard Deviation of Differences is 0.036. The ANOVA test finds no significant difference between the three products, with p = 0.054, which is close to p = 0.05. We also compare in the Rhine River the Sentinel-6A FFSAR and UFSAR results of Fig. 5(a). We find no significant difference in STDD between 140 Hz-FFsamp and 140 Hz-FFsamp with p-value: 0.78, Mean Difference is −0.003 and the Standard Deviation of Differences is 0.017. There is no significant difference between 140 Hz-FFsamp and 20 Hz-EUM with p-value: 0.68. Their Mean Difference is 0.012 and the Standard Deviation of Differences is 0.055. The ANOVA test also finds no significant difference between the three products, with p = 0.75.

4.2. Elbe estuary and coastal zone

High STDDs are expected in estuaries and tidal rivers between altimeter-derived and in-situ water levels, due to land contamination, currents and river flow. The along-track data have been binned. For the four Sentinel-3 tracks selected in the vicinity of a gauge, the STDD between the binned water level heights and the corresponding tide gauge varies strongly along the track, see Fig. 8. The smallest STDDs are found near the navigation channel (red star) and far from the tidal flats. We use as VG the altimeter point with the smallest STDD along each track. Mean and median of the STDD at the four VGs are seen in Tables 6 and 7. Of the HY products, the HYDTU product performs best, with a mean STDD of 0.95 m. Overall, FFSAR 80 Hz with Samp and FFSAR 640 Hz with Ocog give the best performance, both with a STDD smaller than 0.6 meters (0.42 m and 0.52 m in Table 7. The radargrams are highly variable in the tidal flats, see the radargrams for two epochs in Ottendorf (Fig. 8). The tidal range in the Elbe has a total amplitude of about four meters, as seen in time-series of water anomalies in Fig. 6(d). These large discrepancies have been ascribed to both tidal model error and local fine scale dynamics. With FFSAR the results are similar if the same posting rate and retracker are used. The T-test and the ANOVA-test analysis applied to Sentinel-6 show that the STDD of UFSAR and FFSAR against in-situ data do not differ significantly in Fig. 5(c). The p-value is 0.234 for AVLsamp20Hz and FFsamp80Hz with Mean Difference (FFsamp80Hz - AVLsamp20Hz) of 0.168 and Standard Deviation of Differences 0.226.

For the analysis in the coastal zone, for the comparison of UFSAR and FFSAR we have selected two stations in the North Sea, Wittdün (TGWD) and Wangerooge (TGW2), and two stations in the Baltic, Warnemünde and Sassnitz. We apply the overpass method, where all points in a given radius around each in-situ station are averaged to build the altimetric time-series. The radius selected is 5 km. Fig. 5(d) and Tables 8 and 9 show that of the Hydrocoastal products, the HYTUM and HYESA 20 Hz products perform the best, with a mean STDD of 0.06 m (Table 8). The best performance overall is obtained with the UFSAR retracked with SAMOSA+ (AVLsamp). In FFSAR the mean STDD is 0.08 m with the SAMOSA+ retracker, while it is higher with the OCOG and PTR retrackers (Table 9). Further on, we investigate the behaviour of data along track with the binning method. Ten stations and three different methods to build the statistics are used, they are: (1) minimum STDD along track, (2) mean and median along-track and (3) last 20 km from the coast. Using six in-situ stations in the German Bight (BORJ, LHAW, HELG, TGME, TGWD, TGW2) and four in the Baltic (LTKI, SASS, SCHL, WARN) we detect a standard deviation increase in the last 4–5 kilometers near the coast. By choosing the minimum STDD along the track, the DTU retracker gives the smallest median over the stations (0.112 m). By choosing the median STDD the STARS retracker gives the smallest median over the stations (0.172 m). In the coastal zone we compare the Sentinel-3 FFSAR and UFSAR results shown in Fig. 5(d). We find a significant difference in STDD between 80z-FFsamp and 20 Hz-AVLsamp with p-value: 0.007. The Mean Difference (AVLsamp20Hz - FFsamp80Hz) is −0.022 and the Standard Deviation of Differences is 0.0067. Instead

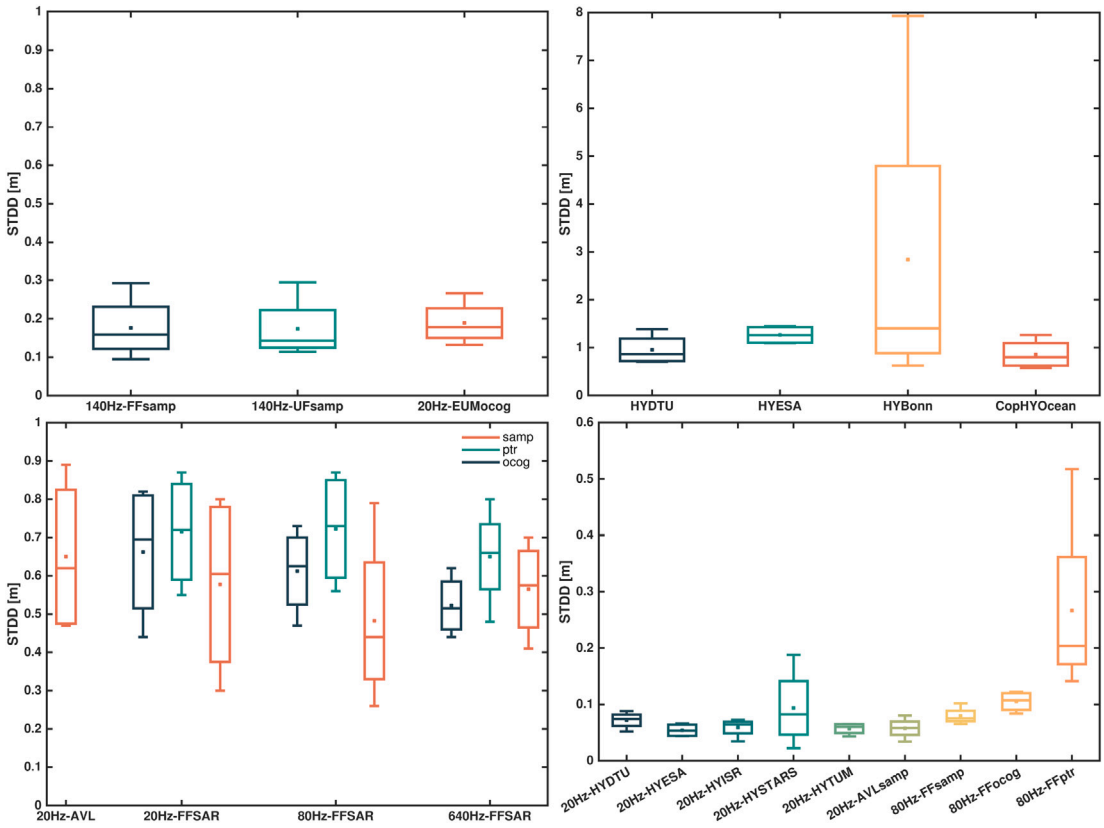


Fig. 5. Boxplots of STDD between in-situ and (a) Sentinel-6A altimetry in River Rhine at 4 VGs of FFSAR and 20 Hz Copernicus Thematic products, (b) Sentinel-3 altimetry in the Elbe estuary at 4 VGs of Hydrocoastal products and CopHYOcean at 20 Hz, (c) Sentinel-3 altimetry in the Elbe estuary at 4 VGs of Earth Console 20 Hz and FFSAR, (d) Sentinel-3 in the coastal zone at 9 VGs of UFSAR and FFSAR products.

the two UFSAR products of Hydrocoastal 20 Hz-AVLsamp and 20 Hz-HYTUM have no statistically significant difference in STD (p-value: 0.923). The mean difference (HYTUM20Hz - AVLsamp20Hz) is 0.0006 and the Standard Deviation of Differences is 0.011.

4.3. Lakes

Fig. 9, top shows the STDD between water level heights binned at 20 Hz and gauges in the Lake of Constance along two tracks of Sentinel-3. The results of FFSAR and HYDTU are similar. The heights are contaminated near land along track A156 (left) and less so along track B350 which is in the middle of the lake. Due to the track shifting, the contamination along track A156 is larger in the second epoch selected and the STDD varies between 20 and 6 cm depending on the distance to the shore. Instead, along track B350 the STDD is 6 cm until 1–2 km from the coast. Fig. 9 (bottom) shows the FFSAR radargrams for two different epochs. Over the interval 2016–2024 the STDD is 9 cm Fig. 12(e) and Fig. 12(f). Unlike the Elbe, where the influence of the ocean tide is more significant, there is less variability than in the radargrams of two epochs in Fig. 8, since the water level does not change significantly in the absence of tides. The reason for the observed change in radargrams could be the wind speed and weather conditions.

5. Discussion

The goal of this study is to compare over various targets the accuracy of the water level derived from Sentinel-3 and Sentinel-6 satellite nadir-altimetry in UFSAR and FFSAR processing. Several papers discuss results in critical areas together with modifications to the original FFSAR processing algorithm (Egido and Smith, 2017), including applications in the coastal zone and canals Kleinherenbrink et al. (2020) and in small reservoirs Domingo et al. (2025). FFSAR is expected to improve water level estimation and to become the standard processing in future missions. Different choices of along-track windowing methods, coherent integration times, and multi-looking strategies were suggested for specular and non-specular surfaces Amraoui et al. (2024), reflecting the trade-off between spatial resolution and noise levels. High resolution, which is crucial over specular surfaces to identify small structures, is not critical over the open ocean, where the dominant factors are speckle noise and sea surface motions. In this work we apply the same data processing and comparable validation methods to the four types of water targets: rivers, lakes, estuaries, and coasts. We compare, separately for Sentinel-3 and Sentinel-6, the results obtained from in-house products, external standard products, and project-specific products. For completeness, in this chapter, after summarizing the results of Section 4, we discuss, for specular surfaces, the differences between these results and those obtained from an alternative processing of L1A data based on single echoes over small lakes and rivers. Finally we compare our results with early findings from the SWOT swath-altimetry mission for all four types of water targets.

5.1. Comparison of water levels derived from FFSAR and UFSAR

A first result from Section 4 concerns the accuracy of FFSAR and UFSAR-derived water levels. Using the Hydrocoastal database, we compared several UFSAR processing schemes, from L1A to L1B and from L1B to L2. Depending on the water body considered, the agreement between altimetry-derived water levels and in-situ data varies, and in all cases FFSAR performs better than UFSAR. It was also shown that, although the Hydrocoastal products are valuable, compared to official products the improvement is limited. Instead, the application of the FFSAR processing scheme is more promising. In particular, the in-house implemented

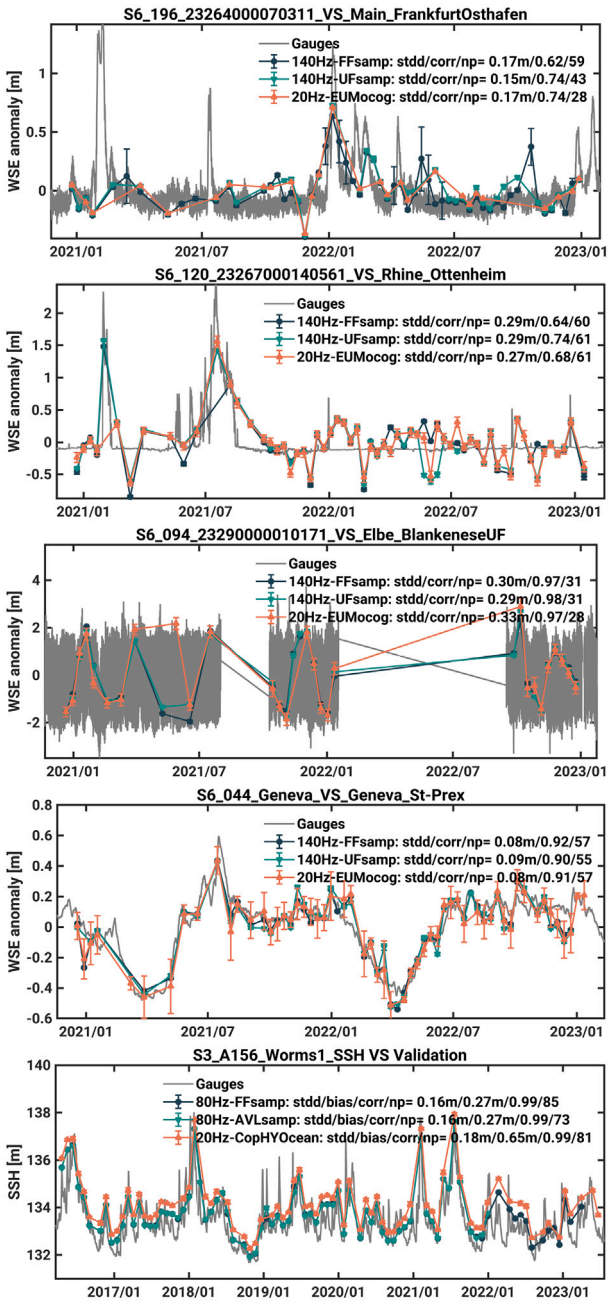


Fig. 6. Time-series from Sentinel-6A (first four from top) in Frankfurt (River Main), Ottenheim (Rhein), Blankenese (Elbe), Lake Geneva and from Sentinel-3 in Worms (Rhein).

FFSAR-WK algorithm in the spatial domain is preferable to the originally implemented FFSAR-BP algorithm in the time domain. Compared with UFSAR, the practical advantages of FFSAR are a higher posting rate and a higher along-track resolution of the water-surface elevation.

A second result from Section 4 is that the accuracy of the retrieved water level depends on several factors: the retracking algorithm, the method of building the time-series, the distance from the in-situ station, the orientation of the tracks relative to the water body and the temporal variability of the water level. The comprehensive HYDROCOASTAL UFSAR analysis in Tables 1 to Table 5 compares state of art, innovative processing and post-processing alternatives providing a synthesis of the UFSAR results. For inland waters using UFSAR, we find that within the HYDROCOASTAL products the DTU product performs better than the others and that the accuracies of the L3 and L2 data differ (Table 3). Concerning the retracking algorithm, the SAMOSA+ retracker achieves similar accuracy in both FFSAR and UFSAR processing (Table 4) and is overall the best-performing retracker. The SAMOSA+ retracker, used in EarthConsole and implemented in our in-house processing, was previously applied to FFSAR processing of CryoSat-2 in Kleinherenbrink et al. (2020). Once the retracker and processing scheme are selected, the accuracy of the water level is primarily driven by the orientation of the track and by the applied slope correction. With tracks parallel to the river, the reduced number of passes available and the application of a static slope correction reduce the accuracy. At Worms and Mannheim, the STDD varies between 18 and 21 cm, compared to a STDD in Mainz of 9–11 cm. The use of a time-varying slope would reduce the STDD of the water height compared to in-situ, however, the time-variable slope along the river can be used in nadir-altimetry only at very few locations when in-situ data are available. As we discuss in Chen et al. (2025), a constant average slope is an acceptable approximation when the real slope does not undergo significant changes. This is not always the case, for example, due to waterfalls, riffles, and pools, significant changes in slope with time cause a 16–24 cm bias of WSE.

The results show that the good performance of the results of FFSAR relative to UFSAR is related to its longer coherent integration time, which generates clearer waveforms and radargrams. To illustrate the differences between the radargrams, Fig. 10 presents FFSAR radargrams for the river reach between Mainz and Speyer. There is a bright signal peak on the radargram at locations where the river is at nadir. The radargram contains a clean signal of the river segment at increased cross-track distances. The FFSAR radargram in Fig. 10 (top left) of 18th April 2018 includes the eight VGs between Mainz and Speyer. Between 49.3° and 49.7° latitude the Sentinel-3A track intersects the river at the eight locations. Also at higher latitudes the river is still well visible even if the distance from nadir is tens of kilometers. Along with the coherent integration time, the along-track resolution also plays a role in resolving small water targets such as reservoirs and narrow rivers, thus the 300 m resolution of UFSAR is a limitation for applications over inland waters and in the coastal zone.

The results show that differences between FFSAR and UFSAR time-series also depend on water body type. Over large lakes, the accuracy of WSE does not differ significantly. The radargrams clearly identify areas with disturbances near the coast. In that zone, the selection of posting rate and retracker is important for both FFSAR and UFSAR results. The SAMOSA+ algorithm retracker is known for its high performance in coastal and inland and is identified as the most suitable retracker also in our study. We select a posting rate of a minimum of 80 Hz to distinguish small features in the radargram and to avoid the smearing of the signal. Over inland waters, we found a bias of around 40 cm relative to in-situ data in the land Thematic products, whereas the in-house FFSAR processing using the SAMOSA+ retracker is not biased. Based on our results, we recommend in coastal zones and estuaries, a FFSAR posting rate of 80/140 Hz. A pre-selection of waveforms based on misfit and other criteria to reduce the geophysical parameter noise was not investigated.

In summary, our results indicate that the FFSAR combined with the SAMOSA+ physical retracker is likely to provide the highest accuracy and the largest number of valid observations across all target types, with mean STDD values smaller than 15 cm in rivers, 8 cm in lakes, 40 cm in estuaries, and 10 cm at the coast (Table 10). One main advantage of FFSAR is the large number of samples available, which enables more effective data screening. However, the improvement in accuracy of FFSAR and UFSAR at the same posting rate and with the same retracker is smaller than 5 %, except for widths smaller than 100 m, water surfaces smaller than 1 km^2, and coastal regions where the contribution of FFSAR is relevant.

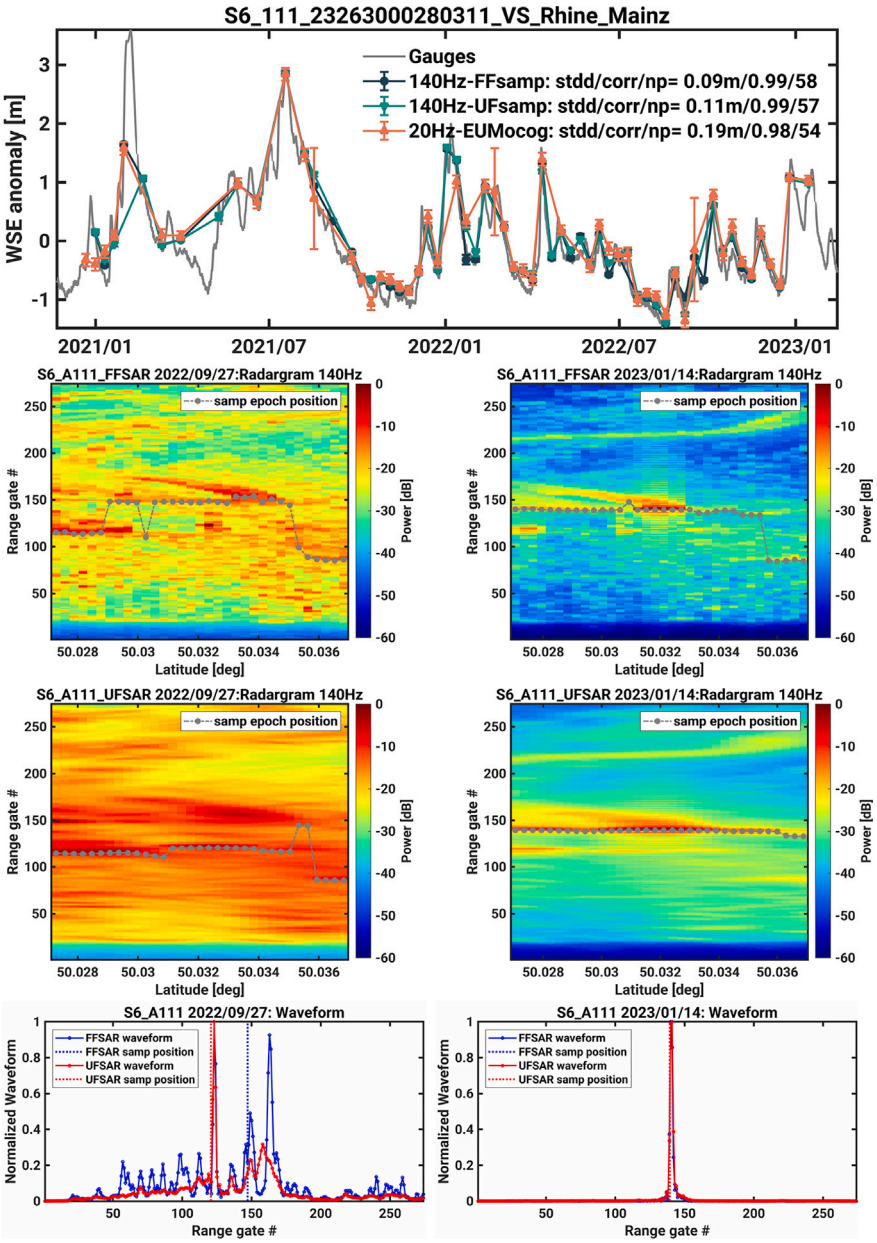


Fig. 7. River Rhine: Sentinel-6A time-series and 140 Hz FFSAR and UFSAR and 20 Hz UFSAR radargrams, waveform collected at mid-river location (latitude 50.0321).

5.2. Analysis of temporal coherence in FFSAR processing

Based on Equation Eq. (2), we estimate the coherence of N consecutive complex single-look waveforms contained in each multi-looked waveform at posting rates of 80, 500, and 1024 Hz (Eq. 11 in Amraoui et al. (2024)). The resulting coherence values under different surface and illumination times are depicted in Figure S5, using Sentinel-3A data from track 156 on April 18, 2018.

$$c_i = \frac{|\sum_{n=0}^{N-1} s_k exp(j\ \ arg(s_k))|^2}{N \sum_{n=0}^{N-1} |(s_k)|^2} \tag{2}$$

The coherence c_i is defined as the ratio between a complex summation and a power summation of individual single-looks (s_k). The value of the coherence is equal to 1 for single-looks with the same phase and can decrease when the phase is not the same. The phase can change due to waves, wind or river slope. We have investigated the temporal decorrelation for different posting rates and illumination times in different water bodies considered in this study. The coherence is maximal in the pond and decreases for rivers, lakes and oceans in that order. For a given water body, it depends on posting rate and illumination time. For the river, the highest coherence of 0.2 is found with a posting rate of 500 Hz, and it is lower for both 80 Hz and 1024 Hz.

In the pond, the coherence remains above 0.9 at high posting rates (500 and 1024 Hz) across all illumination times. At the low posting rate of 80 Hz, however, the coherence drops below 0.6, though it shows some recovery under both small and high illumination times. In oceans and large lakes, wind or waves corrupt the phase of the return signal, resulting in coherence values below 0.2. For the river target, coherence is higher than in the ocean but remains below 0.3. The maximum coherence observed in the river is approximately 0.2, occurring at a posting rate of 500 Hz, while lower values are recorded at both 80 Hz and 1024 Hz. This reduction is attributed to signal decorrelation caused by the slope of the river. Additionally, as the dimensions of the lake decrease, the coherence tends toward higher values.

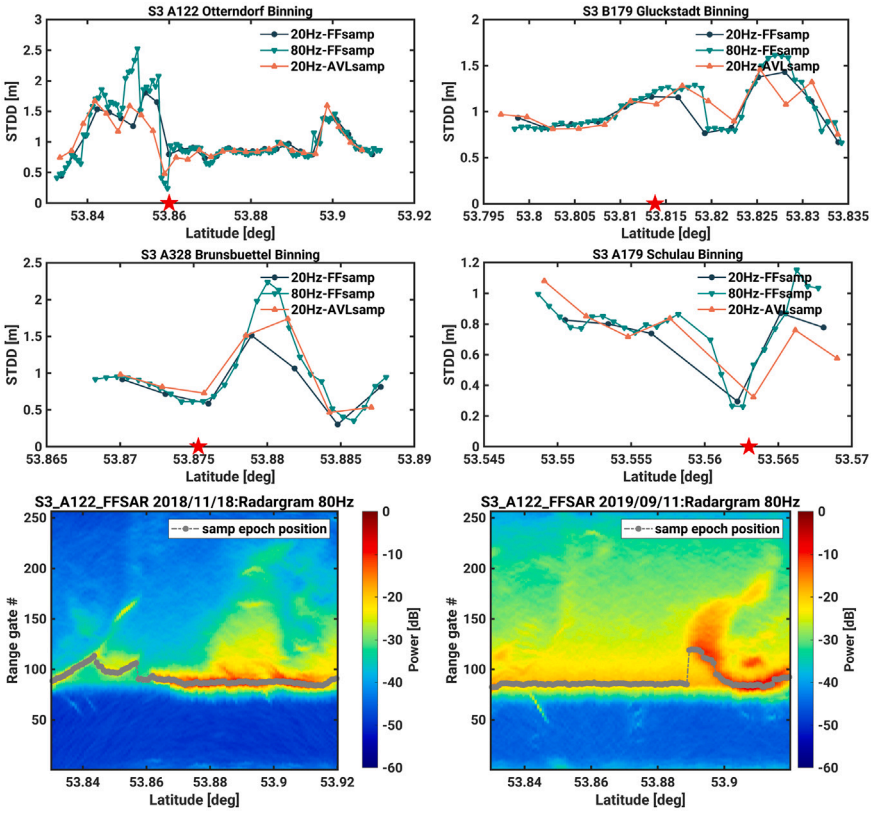


Fig. 8. Elbe Estuary: binned STDD along-track and FFSAR radagrams of FFSAR at Ottendorf, stars indicate the navigation channel of maximum depth.

Table 6
Sentinel-3 Elbe: Mean and median of STDD of in-situ (in meters) and altimeter time-series from Hydrocoastal, 4 VGs, binned method, Fig. 5(b).

STDD	HYDTU 20 Hz	HYESA 20 Hz	HYBonn 20 Hz	CopHYOce 20 Hz
Median	0.862	1.259	1.401	0.798
Mean	0.953	1.263	2.838	0.857

Table 7
Sentinel-3 Elbe: STDD of in-situ (in meters) and altimetric time-series from FFSAR compared to AVLsamp, 4 VGs, Binned, Fig. 5(c).

STDD	AVLsamp 20 Hz	FFsamp 20 Hz	FFsamp 80 Hz	FFocog 80 Hz	FFsamp 640 Hz	FFocog 640 Hz
Median	0.62	0.61	0.44	0.63	0.58	0.52
Mean	0.65	0.58	0.42	0.61	0.57	0.52

Table 8
Sentinel-3 Coastal: Mean and median of STDD of in-situ (m) and altimetric time-series from HY, 4 VGs, Overpass, Fig. 5(d).

STDD	HYDTU 20 Hz	HYESA 20 Hz	HYISR 20 Hz	HYBonn 20 Hz	HYTUM 20 Hz
Median	0.072	0.059	0.065	0.091	0.059
Mean	0.075	0.057	0.065	0.097	0.057

Table 9
Sentinel-3 Coastal: Mean and median of STDD of in-situ (in meters) and altimetric time-series from HY and FFSAR, Coast, 4 VGs, Overpass, Fig. 5(d).

STDD	AVLsamp 20 Hz	FFSARsamp 80 Hz	FFSARocog 80 Hz	FFSARptr 80 Hz
Median	0.057	0.078	0.123	0.211
Mean	0.057	0.080	0.112	0.267

Table 10
Summary of STDD between Sentinel-3 UFSAR/FFSAR and gauges for different surfaces with median (in meters), Tables 3, 7 and 9.

	AVLsamp	FFSARsamp	Surface
Median	0.06 (20 Hz)	0.08 (80 Hz)	Coast (dc>5 km)
Median	0.62 (20 Hz)	0.44 (80 Hz)	Estuaries
Median	0.21 (20 Hz)	0.16 (80 Hz)	River

dc: distance to coast.

5.3. Comparison of water levels derived from FFSAR and PISA

Alternatively to the FFSAR processing, other processing methods are used. Here, we consider the Precision Inland Surface Altimetry (PISA) processing (Abileah and Vignudelli, 2021) and analyze the differences between PISA and FFSAR radargrams and time-series. PISA exploits specular echoes, assumes quasi-specular inland waters and is suited to water widths of 100 m or greater. Its optimum coherent integration time is the duration of the nadir looking over the water surface. PISA processes individual bursts and coherently sums the 64 individual pulses contained in Sentinel-3 bursts, producing one estimate per burst with a posting of 89 m along-track. The Hamming window is applied, and the retracker used is SINC. For each burst, PISA outputs waveforms, range, and surface elevations derived from those ranges.

Fig. 10 (top left) provides an example of a PISA radargram. The differences between PISA and FFSAR are analyzed in the two case-studies.

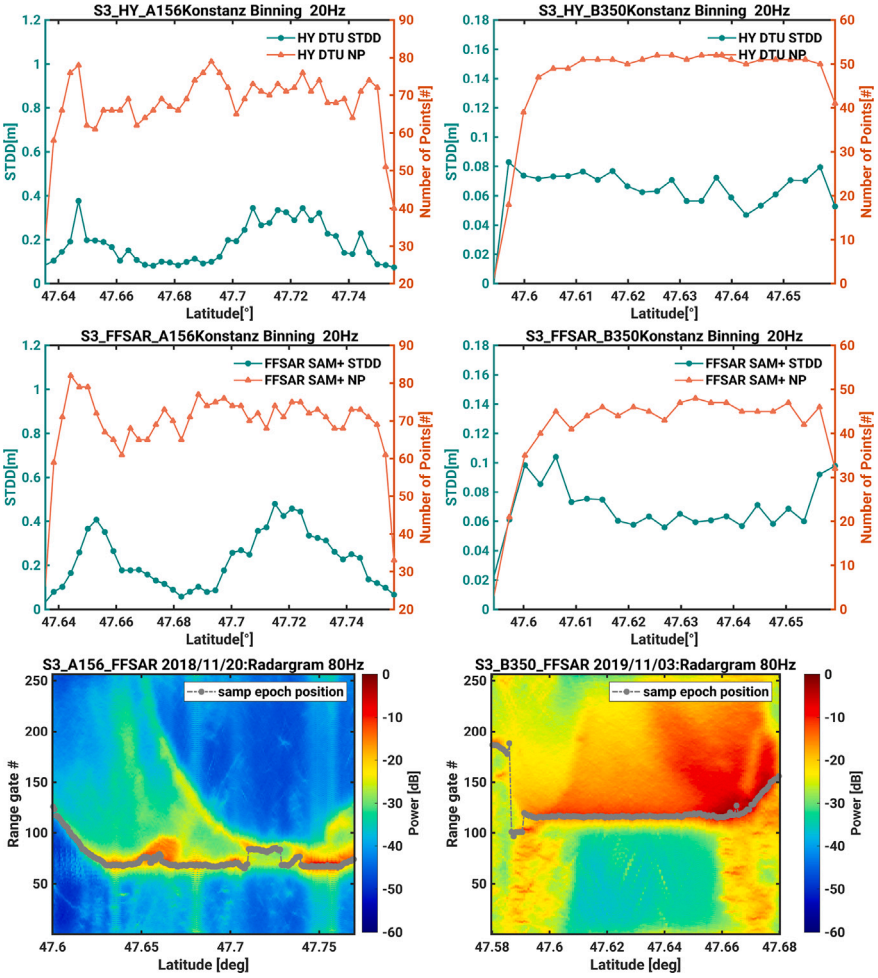


Fig. 9. Lake of Constance, Sentinel-3: Standard deviation differences (STDD) between time-series binned at 20 Hz along-track with in-situ time-series from UFSAR (top) and FFSAR (second from top) for pass A156 (left) and pass B350 (right). FFSAR 80 Hz radargrams at one epoch for each track (below) with land contamination.

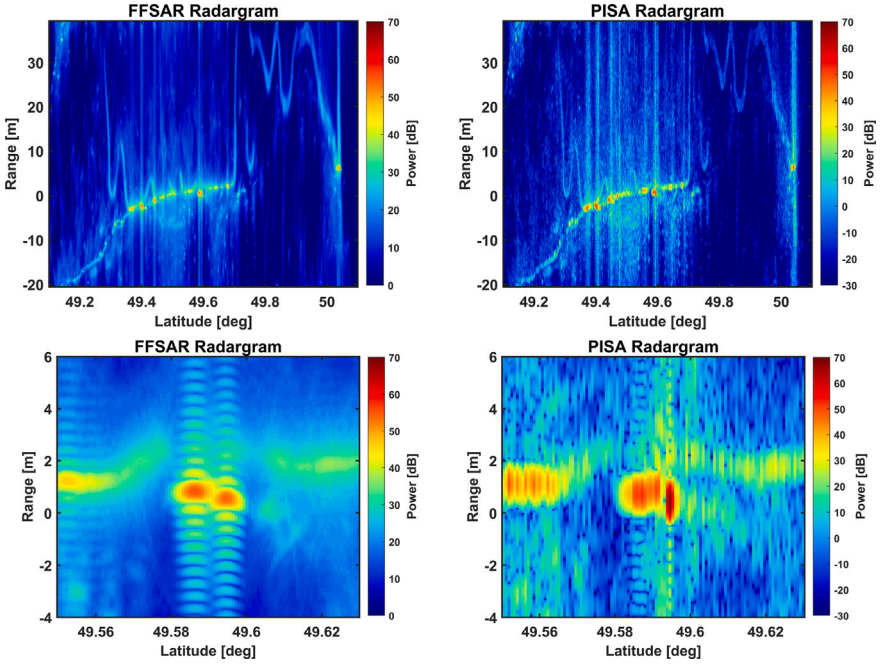


Fig. 10. Radargram FFSAR and PISA at 80 Hz with zero padding 469 and Hamming, between Mainz and Maxau of Sentinel-3A (top) and on a pond, date is 18-04-2018 (bottom).

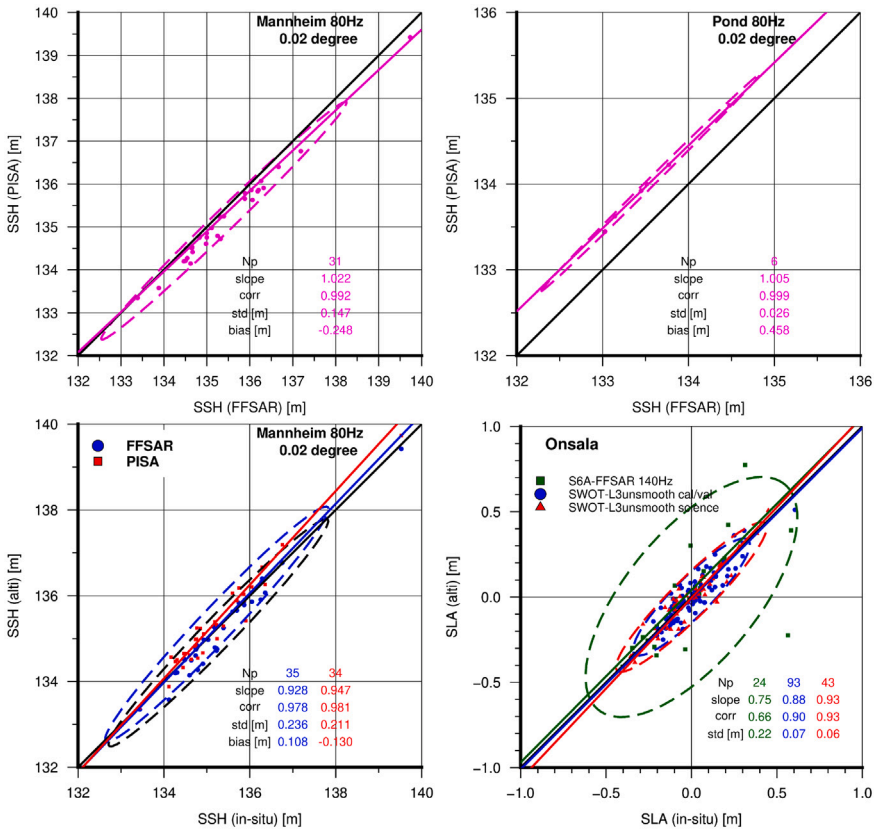


Fig. 11. Scatterplot of SSH FFSAR against SSH PISA in in-land water, in Rhine (a) and in polder (b), SSH FFSAR and PISA against in-situ measurements in Mannheim (c), sea level anomaly near the Onsala gauge from SWOT and nadir-altimetry against in-situ. Distance to the coast is 2 km (d).

The first case-study concerns the Rhine River near the Mannheim in-situ gauge and includes both altimetric and in-situ time series. The altimetric time series are constructed from observations near the Mannheim gauge and compared with the in-situ record. The agreement between altimeter and in-situ time-series is within 25 cm (STDD) for both altimeter products (Fig. 11c). The difference between the time-series is ascribed to land contamination and to the slope between the in-situ and the altimeter observations, which is not accounted for. We observe a different bias, 11 cm in FFSAR and −13 cm in PISA. The STDD of the two altimetric time-series is 15 cm, with a bias of −25 cm (Fig. 11c). The second case study concerns a pond with a diameter of 140 m located between latitudes 49.594 and 49.595, for which only altimeter data are available. On 18th April 2018 Sentinel-3 overflies the pond, providing an ideal case for comparing PISA to FFSAR. In PISA, one burst captures the specular flash, and since the pond is close to a Fresnel zone dimension (190 m), little echo power is observed from off-nadir. By contrast, FFSAR sums power also from the Rhine and from other nearby ponds. The PISA and FFSAR radargrams look similar, but a zoomed view shows that PISA localizes the pond better than FFSAR in the radargram in Fig. 10(c) and d. The STDD of the altimetric time-series from FFSAR and PISA is 3 cm with a bias of 45 cm (Fig. 11b).

5.4. Comparison of water levels derived from FFSAR and SWOT

Finally, we compare the accuracy of water levels derived from FFSAR processed nadir-altimetry with those derived from the Surface Water and Ocean Topography (SWOT). We aim to investigate whether SWOT provides more accurate water levels than nadir-altimetry and which types of errors may influence the difference in accuracy between SWOT and FFSAR.

In a quantitative accuracy comparison between SWOT and FFSAR, both numerical differences and differences in the physical mechanisms of their errors should be considered. Indeed, the error budget varies between the altimeters. For nadir altimeters, inland-water level accuracy is commonly affected by land contamination, off-nadir bright targets, atmospheric path delays, and instrumental noise. Along-track Sea Surface Height errors are typically on the order of 2–5 cm over open water, with errors largely uncorrelated along the track (Desai, 2018). In contrast, SWOT measurements are influenced by additional systematic effects related to interferometric geometry. The Ka-band Radar Interferometer (KaRIn) is sensitive to platform attitude and baseline configuration. Baseline roll angle and baseline length errors introduce spatially correlated noise across the swath, particularly in the cross-track direction (Dibarboure et al., 2022). Over inland waters, residual systematic errors on the order of 3–6 cm have been reported (Dibarboure et al., 2022). The raw cross-track error can be large, potentially exceeding 10–20 cm at the edge of the swath before calibration. Unlike nadir altimetry, these errors are not white noise but are spatially correlated in the cross-track direction and vary along the ground track. However, after calibration and, when combined with multiple nadir altimeters, these errors can be significantly reduced, with post-processed RMS errors falling into the 1–4 cm range (Desai, 2018; Peral et al., 2024).

As for the FFSAR data, we compare SWOT-derived and in-situ water levels for the different types of surfaces rivers, estuaries, and lakes. The time-series of SWOT against the in-situ data are shown in Fig. 12. In rivers and estuaries, we use the High Resolution (HR) SWOT-PIXC products. During the Cal/Val phase, SWOT achieves high accuracy over the Rhine River, with STDD values of 5 and 7 cm relative to the Worms and Mainz gauge stations, respectively (Fig. 12a and b). By comparison, the best STDD obtained with FFSAR is 9 cm (Fig. 3). The accuracy of SWOT

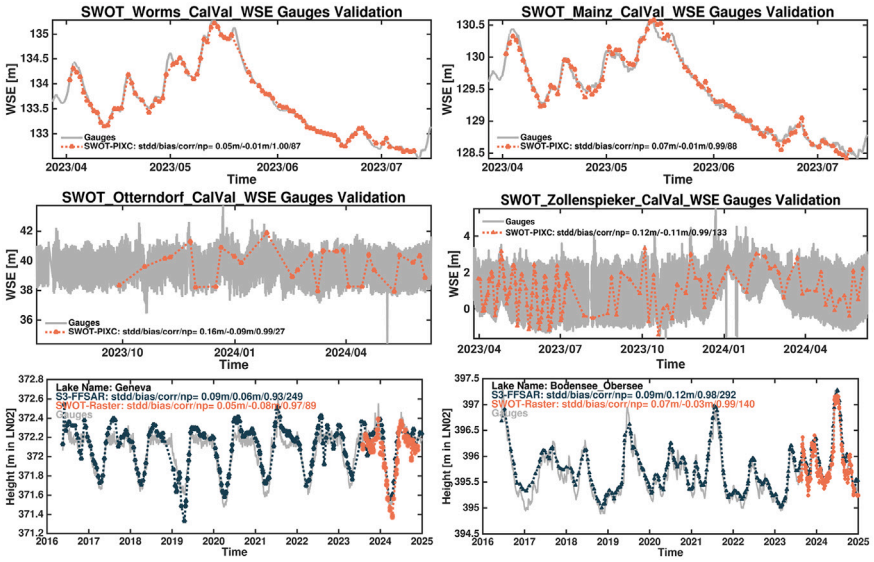


Fig. 12. Time-series of SWOT in rivers from SWOT-PIXC and in lakes from SWOT-Raster. From top to bottom: in rivers near in-situ gauge of Mainz (Rhine), Worms (Rhine), Otterndorf (Elbe), Zollenspieker (Elbe) and in lakes averaged over lake Constance and Geneva.

over the Rhine River is consistent with results reported for other inland regions (Maubant et al., 2025; Patidar et al., 2025). In the Elbe estuary, SWOT reaches an STDD of 16 cm relative to the Ottendorf gauge (Fig. 12c), whereas Sentinel-3A yields an STDD of 50 cm at the same station (Fig. 8). Upstream in the Elbe tidal river, the river dynamics with interacting tidal currents and discharge may explain the higher STDD of 26 cm at the Zollenspieker gauge in Fig. 12(d). This performance is consistent with results reported for other estuarine regions (Lichtman et al., 2025). In lakes, we use the SWOT-Raster product. For comparison with a given gauge, the time series is computed from the raster data using the median value within the lake mask. In the large Lake Geneva and Lake Constance, the STDD with gauges St-Prex and Romanshorn is 5–7 cm with SWOT (Fig. 12e) and Fig. 12(f), compared with 9 cm for Sentinel-3 FFSAR (Fig. 9), which is in agreement with Bazzi et al. (2025). In coastal areas, we use the L3 Low Resolution (LR) unsmoothed product. For comparison with the Onsala gauge station, the altimeter data are selected at 2 km from the coast. The STDD is low for SWOT data from both the Cal/Val and science phases (6–7 cm), whereas it is higher for Sentinel-6A FFSAR data (22 cm; Fig. 11(d). The smaller and more elongated ellipses for SWOT indicate stronger consistency with the in-situ SLA, while the broader ellipse for Sentinel-6A FFSAR reflects higher variability and weaker correlation. This performance is consistent with results reported for other coastal regions (Turki et al., 2025). All results in Fig. 12 show a higher accuracy for SWOT than for nadir-altimeters. However, the smaller standard deviation against the gauges does not necessarily indicate a higher accuracy of the measurement itself. The methodology of comparison plays a role and the smaller standard deviation is also driven by the large number of observations that are averaged to compute the SWOT time-series.

The comparison between FFSAR nadir altimetry and SWOT shows the advantage of two dimensional mapping at high spatial resolution. Nadir altimeters may perform better in regions of very low SLA variability and can help constrain SWOT maps. Off-nadir FFSAR processing (Chen et al., 2025) allows extending nadir altimetry to a two dimensional surface over small selected river targets to obtain a similar coverage as SWOT.

6. Conclusion

We have investigated the advantage of the newly emerging FFSAR processing scheme against the SAR delay/Doppler processing. First we observe that the FFSAR combined with the SAMOSA+ physical retracker is likely to provide the highest accuracy and the largest number of observations over all targets. Values for the STDD based on the achieved results, indicate a mean STDD smaller than 15 cm in rivers, 8 cm in lakes, 40 cm in estuaries and 10 cm at the coast. Compared to the UFSAR results, the improvement in accuracy of FFSAR and UFSAR at the same frequency and with the same retracker is smaller than 5 %. However, due to its higher resolution FFSAR is important for small targets, such as rivers with widths smaller than 100 km, water surfaces smaller than 1 km^2 and areas near the coast. In larger targets FFSAR increases the number of measurements and thus their accuracy. We anticipate that the applications of FFSAR will develop rapidly in inland and coastal regions thanks to the reduced computing time needed with the WK algorithm.

CRediT authorship contribution statement

Luciana Fenoglio: Conceptualization, Formal analysis, Funding acquisition, Methodology, Software, Supervision, Validation, Writing – original draft. **Jiaming Chen:** Writing – review & editing, Validation, Software, Methodology, Data curation. **Stefano Vignudelli:** Writing – review & editing, Validation. **Ron Abileah:** Writing – review & editing, Software. **Elena Zakharova:** Writing – review & editing. **Marco Restano:** Writing – review & editing, Conceptualization. **Jerome Benveniste:** Writing – review & editing. **Jürgen Kusche:** Writing – review & editing.

Open research

The L2 products for Sentinel-3 and Sentinel-6 processed in FFSAR mode can be provided upon request. The time series of water level heights in inland water bodies are part of the DETECT database $B01 - DETECT - DIWASAR$ and are accessible via the DETECT project website as single time-series and in netcdf files https://detect-z03.geoinformation.net/map/. The netcdf file B01-DETECT-DIWASAR_RWQ_FN_V1.0_16-24_20250704.nc contains water levels at nadir-altimetry virtual gauges.

Funding

Support was partly provided by the European Space Agency projects Hydrocoastal (https://www.satoc.eu/projects/hydrocoastal/docs.html)

and 4D BALTDYN (https://4dbaltdyn.albavalor.es) projects and partly by the Deutsche Forschungsgemeinschaft (DFG, German Research Foundation) in the DETECT-B01-Collaborative Research Center 1502/1-2022-450058266 (https://sfb1502.de).

Declaration of competing interest

The authors declare that they have no known competing financial interests or personal relationships that could have appeared to influence the work reported in this paper.

Acknowledgements

The authors gratefully acknowledge the Jülich Supercomputing Centre (https://www.fz-juelich.de/jsc) for providing computing time on JUWELS through the Gauss Centre for Supercomputing for project B01-FFSAR. The ESA Network of Resources supported this study with computing time. We acknowledge the National Hydrological Agency and Waterways and Shipping Administration (BfG) for the in-situ water level data and the European Space Agency, EUMETSAT and CNES for the altimeter data used in this study.

Appendix A. Supplementary data

Supplementary data for this article can be found online at doi:10.1016/j.jhydrol.2026.135681.

Data availability

Level 2 in-house data are available on request, time-series are available, see open research section.

References

Abileah, R., Vignudelli, S., 2021. Precise inland surface altimetry (PISA) with nadir specular echoes from sentinel-3: algorithm and performance assessment. Remote Sens. Environ. 264, 112580. https://doi.org/10.1016/j.rse.2021.112580

Abulaitijiang, A., Andersen, O.B., Stenseng, L., 2015. Coastal sea level from inland cryosat-2 interferometric SAR altimetry. Geophys. Res. Lett. 42, 1841–1847. https://doi.org/10.1002/2015GL063131

Altenau, E.H., Pavelsky, T.M., Durand, M.T., Yang, X., Frasson, R.P.D.M., Bendezu, L., 2021. The surface water and ocean topography (SWOT) mission river database (SWORD): a global river network for satellite data products. Water Resour. Res. 57, e2021WR030054. https://doi.org/10.1029/2021WR030054

Amraoui, S., Guccione, P., Moreau, T., Alves, M., Altiparmaki, O., Peureux, C., Recchia, L., Maraldi, C., Boy, F., Donlon, C., 2024. Optimal configuration of omega-kappa FF-SAR processing for specular and non-specular targets in altimetric data: the sentinel-6 Michael freilich study case. Remote Sens. 16, https://doi.org/10.3390/rs16061112

Archer, M., Wang, J., Klein, P., Dibarboure, G., Fu, L.L., 2025. Wide-swath satellite altimetry unveils global submesoscale ocean dynamics. Nature 640, 691–696. https://doi.org/10.1038/s41586-025-08722-8

Bazzi, H., Baghdadi, N., Ngo, Y.N., Normandin, C., Frappart, F., Cazals, C., 2025. Assessing SWOT interferometric SAR altimetry for inland water monitoring: insights from lake Léman. Front. Remote Sens. 6 (2025), https://doi.org/10.3389/frsen.2025.1572114. https://www.frontiersin.org/journals/remote-sensing/articles/10.3389/frsen.2025.1572114.

Benveniste, J., Cazenave, A., Vignudelli, S., Fenoglio-Marc, L., Shah, R., Almar, R., Andersen, O., Birol, F., Bonnefond, P., Bouffard, J., Calafat, F., Cardellach, E., Cipollini, P., Le Cozannet, G., Dufau, C., Fernandes, M.J., Frappart, F., Garrison, J., Gommenginger, C., Han, G., Høyer, J.L., Kourafalou, V., Leuliette, E., Li, Z., Loisel, H., Madsen, K.S., Marcos, M., Melet, A., Meyssignac, B., Pascual, A., Passaro, M., Ribó, S., Scharroo, R., Song, Y.T., Speich, S., Wilkin, J., Woodworth, P., Wöppelmann, G., 2019. Requirements for a coastal hazards observing system. Front. Mar. Sci. 6, https://doi.org/10.3389/fmars.2019.00348

Biancamaria, S., Lettenmaier, D., Pavelsky, T., 2016. The SWOT mission and its capabilities for land hydrology. Surv. Geophys. 37, 307–337. https://doi.org/10.1007/s10712-015-9346-y

Boergens, E., Dettmering, D., Schwatke, C., Seitz, F., 2016. Treating the hooking effect in satellite altimetry data: a case study along the Mekong river and its tributaries. Remote Sens. 8, https://doi.org/10.3390/rs8020091. https://www.mdpi.com/2072-4292/8/2/91.

Buchhaupt, C., Fenoglio-Marc, L., Dinardo, S., Scharroo, R., Becker, M., 2018. A fast convolution based waveform model for conventional and unfocused SAR altimetry. Adv. Space Res. 62, 1445–1463. https://doi.org/10.1016/j.asr.2017.11.039. The CryoSat Satellite Altimetry Mission: Eight Years of Scientific Exploitation.

Cerbelaud, A., David, C.H., Pavelsky, T., Biancamaria, S., Garambois, P.A., Kittel, C., Papa, F., Bates, P., Tourian, M.J., Durand, M., Frasson, R., Oubanas, H., Simard, M., Schumann, G., Allen, G., Tarpanelli, A., Wongchuig, S., Wade, J., Tom, M., Malaterre, P.O., Gleason, C.J., Crétaux, J.F., Nielsen, K., Elmi, O., Schwatke, C., Scherer, D., Gal, L., Paris, A., Dasgupta, A., Munier, S., Feng, D., Bauer-Gottwein, P., Hossain, F., Yamazaki, D., Kitambo, B., Mischel, S., Bonnema, M., Verma, K., Andreadis, K., Picot, N., Benveniste, J., 2025. Satellite requirements to capture water propagation in earth's rivers. Rev. Geophys. 63, e2024RG000871. https://doi.org/10.1029/2024RG000871.

Chen, J., Fenoglio, L., Kusche, J., 2025. Measuring off-nadir river water levels and slopes from altimeter fully-focused SAR mode. J. Hydrol. 650, 132553. https://doi.org/10.1016/j.jhydrol.2024.132553

Davis, C., 1997. A robust threshold retracking algorithm for measuring ice-sheet surface elevation change from satellite radar altimeters. IEEE Trans. Geosci. Remote Sens. 35, 974–979. https://doi.org/10.1109/36.602540

Desai, S., 2018. SWOT Mission Science Requirements Document, JPL D-61923 Rev B. Technical Report. Available at, Jet Propulsion Laboratory. https://swot.jpl.nasa.gov.

Dibarboure, G., Ubelmann, C., Flamant, B., Briol, F., Peral, E., Bracher, G., Vergara, O., Faugère, Y., Soulat, F., Picot, N., 2022. Data-driven calibration algorithm and pre-launch performance simulations for the SWOT mission. Remote Sens. 14, https://doi.org/10.3390/rs14236070

Dinardo, S., Fenoglio-Marc, L., Buchhaupt, C., Becker, M., Scharroo, R., Joana Fernandes, M., Benveniste, J., 2018. Coastal SAR and PLRM altimetry in German bight and west Baltic sea. Adv. Space Res. 62, 1371–1404. https://doi.org/10.1016/j.asr.2017.12.018

Dinardo, S., Fenoglio-Marc, L., Becker, M., Scharroo, R., Fernandes, M.J., Staneva, J., Grayek, S., Benveniste, J., 2021. A RIP-based SAR retracker and its application in North East atlantic with sentinel-3. Adv. Space Res. 68, 892–929. https://doi.org/10.1016/j.asr.2020.06.004

Domingo, X., Gibert, F., Molina, R., Escorihuela, M.J., 2025. Improved inland water level estimates with sentinel-6 fully focused SAR processing: a case study in the ebre river basin. Remote Sens. 17, https://doi.org/10.3390/rs17030531

Donlon, C.J., Cullen, R., Giulicchi, L., Vuilleumier, P., Francis, C.R., Kuschnerus, M., Simpson, W., Bouridah, A., Caleno, M., Bertoni, R., Rancaño, J., Pourier, E., Hyslop, A., Mulcahy, J., Knockaert, R., Hunter, C., Webb, A., Fornari, M., Vaze, P., Brown, S., Willis, J., Desai, S., Desjonqueres, J.D., Scharroo, R., Martin-Puig, C., Leuliette, E., Egido, A., Smith, W.H., Bonnefond, P., Le Gac, S., Picot, N., Tavernier, G., 2021. The Copernicus sentinel-6 mission: enhanced continuity of satellite sea level measurements from space. Remote Sens. Environ. 258, 112395. https://doi.org/10.1016/j.rse.2021.112395

Egido, A., Smith, W.H.F., 2017. Fully focused SAR altimetry: theory and applications. IEEE Trans. Geosci. Remote Sens. 55, 392–406. https://doi.org/10.1109/TGRS.2016.2607122

Egido, A., Dinardo, S., Ray, C., 2021. The case for increasing the posting rate in delay/Doppler altimeters. Adv. Space Res. 68, 930–936. https://doi.org/10.1016/j.asr.2020.03.014

Ehlers, F., Schlembach, F., Kleinherenbrink, M., Slobbe, C., 2023a. Validity assessment of SAMOSA retracking for fully-focused SAR altimeter waveforms. Adv. Space Res. 71, 1377–1396. https://doi.org/10.1016/j.asr.2022.11.034

Ehlers, F., Slobbe, C., Verlaan, M., Kleinherenbrink, M., 2023b. A noise autocovariance model for SAR altimeter measurements with implications for optimal sampling. Adv. Space Res. 71, 3951–3967. https://doi.org/10.1016/j.asr.2023.02.043

Ehlers, F., Slobbe, C., Schlembach, F., Kleinherenbrink, M., Verlaan, M., 2025. Polygon-informed cross-track altimetry (PICTA): estimating river water level profiles with the sentinel-6 altimeter. Remote Sens. Environ. 316, 114479. https://doi.org/10.1016/j.rse.2024.114479

Fenoglio, L., Dinardo, S., Uebbing, B., Buchhaupt, C., Gärtner, M., Staneva, J., Becker, M., Klos, A., Kusche, J., 2021. Advances in NE-atlantic coastal sea level change monitoring by delay Doppler altimetry. Adv. Space Res. 68, 571–592. https://doi.org/10.1016/j.asr.2020.10.041. 25 Years of Progress in Radar Altimetry.

Gao, Q., Makhoul, E., Escorihuela, M.J., Zribi, M., Quintana Seguí, P., García, P., Roca, M., 2019. Analysis of retrackers' performances and water level retrieval over the ebro river basin using sentinel-3. Remote Sens. 11, https://doi.org/10.3390/rs11060718

Guccione, P., Scagliola, M., Giudici, D., 2018. 2D frequency domain fully focused SAR processing for high PRF radar altimeters. Remote Sens. 10, https://doi.org/10.3390/rs10121943

Halicki, M., Schwatke, C., Niedzielski, T., 2023. The impact of the satellite ground track shift on the accuracy of altimetric measurements on rivers: a case study of the sentinel-3 altimetry on the odra/oder river. J. Hydrol. 617, 128761. https://doi.org/10.1016/j.jhydrol.2022.128761

Hernández-Burgos, S., Gibert, F., Broquetas, A., Kleinherenbrink, M., De la Cruz, A.F., Gómez-Olivé, A., García-Mondéjar, A., I Aparici, M.R., 2024. A fully focused SAR omega-K closed-form algorithm for the sentinel-6 radar altimeter: methodology and applications. IEEE Trans. Geosci. Remote Sens. 62, 1–16. https://doi.org/10.1109/TGRS.2024.3367544

JPL D-56411, Revision C, 2025. SWOT Product Description Document: Level 2 KaRIn High Rate Water Mask Pixel Cloud (L2_HR_PIXC) Data Product. Technical Report, Jet Propulsion Laboratory Internal Document.

Kleinherenbrink, M., Naeije, M., Slobbe, C., Egido, A., Smith, W., 2020. The performance of cryosat-2 fully-focussed SAR for inland water-level estimation. Remote Sens. Environ. 237, 111589. https://doi.org/10.1016/j.rse.2019.111589

Le Gac, S., Boy, F., Blumstein, D., Lasson, L., Picot, N., 2021. Benefits of the open-loop tracking command (OLTC): extending conventional nadir altimetry to inland waters monitoring. Adv. Space Res. 68, 843–852. https://doi.org/10.1016/j.asr.2019.10.031. 25 Years of Progress in Radar Altimetry.

Lichtman, I.D., Bell, P.S., Gommenginger, C., Banks, C., Calafat, F.M., Brown, J., Williams, S.D.P., 2025. Evaluating water levels from the surface water and ocean topography (SWOT) mission in a hyper-tidal coastal and estuarine environment. Earth Space Sci. 12, e2024EA004104. https://doi.org/10.1029/2024EA004104.

Maubant, L., Dodd, L., Tregoning, P., 2025. Assessing the accuracy of SWOT measurements of water bodies in Australia. Geophys. Res. Lett. 52, e2024GL114084. https://doi.org/10.1029/2024GL114084.

Nguyen, T.H., Ricci, S., Boy, F., Piacentini, A., Munier, S., Luque, S.P., Fatras, C., Cassan, L., Rodriguez Suquet, R., 2025. Chained hydrologic-hydraulic for flood modeling by assimilating SAR-derived flood extent and FFSAR-processed altimetry data. J. Hydrol. 663, 134013. https://doi.org/10.1016/j.jhydrol.2025.134013

Nielsen, K., Zakharova, E., Tarpanelli, A., Andersen, O.B., Benveniste, J., 2022. River levels from multi mission altimetry, a statistical approach. Remote Sens. Environ. 270, 112876. https://doi.org/10.1016/j.rse.2021.112876

Normandin, C., Frappart, F., Baghdadi, N., Bourrel, L., Peña Luque, S., Ygorra, B., Kitambo, B., Papa, F., Riazanoff, S., Wigneron, J.P., 2024. First results of the surface water ocean topography (SWOT) observations to rivers elevation profiles in the Cuvette Centrale of the Congo Basin. Front. Remote Sens. 5 (2024), https://doi.org/10.3389/frsen.2024.1466695. https://www.frontiersin.org/journals/remote-sensing/articles/10.3389/frsen.2024.1466695.

Passaro, M., Rose, S.K., Andersen, O.B., Boergens, E., Calafat, F.M., Dettmering, D., Benveniste, J., 2018. ALES+: adapting a homogenous ocean retracker for satellite altimetry to sea ice leads, coastal and inland waters. Remote Sens. Environ. 211, 456–471. https://doi.org/10.1016/j.rse.2018.02.074

Patidar, G., Indu, J., Karmakar, S., 2025. Performance assessment of surface water and ocean topography (SWOT) mission for WSE measurement across India. Geophys. Res. Lett. 52, e2025GL115804. https://doi.org/10.1029/2025GL115804. https://agupubs.onlinelibrary.wiley.com/doi/abs/10.1029/2025GL115804.

Pekel, J., Cottam, A., Gorelick, N.E.A., 2016. High-resolution mapping of global surface water and its long-term changes. Nature 540, 418–422. https://doi.org/10.1038/nature20584

Peral, E., Esteban-Fernández, D., Rodríguez, E., McWatters, D., De Bleser, J.W., Ahmed, R., Chen, A.C., Slimko, E., Somawardhana, R., Knarr, K., Johnson, M., Jaruwatanadilok, S., Chan, S., Wu, X., Clark, D., Peters, K., Chen, C.W., Mao, P., Khayatian, B., Chen, J., Hodges, R.E., Boussalis, D., Stiles, B., Srinivasan, K., 2024. KaRIn, the ka-band radar interferometer of the SWOT mission: design and in-flight performance. IEEE Trans. Geosci. Remote Sens. 62, 1–27. https://doi.org/10.1109/TGRS.2024.3405343

Ray, C., Martin-Puig, C., Clarizia, M.P., Ruffini, G., Dinardo, S., Gommenginger, C., Benveniste, J., 2015. SAR altimeter backscattered waveform model. IEEE Trans. Geosci. Remote Sens. 53, 911–919. https://doi.org/10.1109/TGRS.2014.2330423

Roscher, R., Uebbing, B., Kusche, J., 2017. STAR: spatio-temporal altimeter waveform retracking using sparse representation and conditional random fields. Remote Sens. Environ. 201, 148–164. https://doi.org/10.1016/j.rse.2017.07.024

Rulent, J., Calafat, F.M., Banks, C.J., Bricheno, L.M., Gommenginger, C., Green, J.A.M., Haigh, I.D., Lewis, H., Martin, A.C.H., 2020. Comparing water level estimation in coastal and shelf seas from satellite altimetry and numerical models. Front. Mar. Sci. 7, https://doi.org/10.3389/fmars.2020.549467

Schlembach, F., Ehlers, F., Kleinherenbrink, M., Passaro, M., Dettmering, D., Seitz, F., Slobbe, C., 2023. Benefits of fully focused SAR altimetry to coastal wave height estimates: a case study in the north sea. Remote Sens. Environ. 289, 113517. https://doi.org/10.1016/j.rse.2023.113517

Schröder, S., Springer, A., Kusche, J., Uebbing, B., Fenoglio-Marc, L., Diekkrüger, B., Poméon, T., 2019. Niger discharge from radar altimetry: bridging gaps between gauge and altimetry time series. Hydrol. Earth Syst. Sci. 23, 4113–4128. https://doi.org/10.5194/hess-23-4113-2019

Schwatke, C., Dettmering, D., Bosch, W., Seitz, F., 2015. DAHITI – an innovative approach for estimating water level time series over inland waters using multi-mission satellite altimetry. Hydrol. Earth Syst. Sci. 19, 4345–4364. https://doi.org/10.5194/hess-19-4345-2015

Turki, E., Islam, M., Solano, C.L., Salameh, E., Domingues, M., Mendoza, T., Aouf, L., Froideval, L., Barcelo, D.G., Laignel, B., Carbonniere, A., Frappart, F., 2025. On the use of SWOT altimetry data for monitoring coastal hydrodynamics. Int. J. Appl. Earth Obs. Geoinf. 145, 104982. https://doi.org/10.1016/j.jag.2025.104982. https://www.sciencedirect.com/science/article/pii/S1569843225006296.

Verger-Miralles, E., Mourre, B., Gómez-Navarro, L., Barceló-Llull, B., Casas, B., Cutolo, E., Díaz-Barroso, L., d'Ovidio, F., Tarry, D.R., Zarokanellos, N.D., Pascual, A., 2025. SWOT enhances small-scale eddy detection in the Mediterranean Sea. Geophys. Res. Lett. 52, e2025GL116480. https://doi.org/10.1029/2025GL116480.

Villadsen, H., Deng, X., Andersen, O.B., Stenseng, L., Nielsen, K., Knudsen, P., 2016. Improved inland water levels from SAR altimetry using novel empirical and physical retrackers. J. Hydrol. 537, 234–247. https://doi.org/10.1016/j.jhydrol.2016.03.051

Wang, J., Pottier, C., Cazals, C., Battude, M., Sheng, Y., Song, C., Sikder, M.S., Yang, X., Ke, L., Delhoume, M., Gosset, M., Oliveira, R.R.A., Grippa, M., Girard, F., Allen, G.H., Xu, X., Zhu, X., Biancamaria, S., Smith, L.C., Crétaux, J.F., Pavelsky, T.M., 2025. The surface water and ocean topography mission (SWOT) Prior Lake database (PLD): lake mask and operational auxiliaries. Water Resour. Res. 61, https://doi.org/10.1029/2023WR036896